

## GZK Photons as Ultra High Energy Cosmic Rays

Graciela B. Gelmini<sup>a,b</sup>, Oleg E. Kalashev<sup>c</sup> and Dmitry V. Semikoz<sup>d,b</sup>

<sup>a</sup> Department of Physics and Astronomy, UCLA, Los Angeles, CA 90095-1547, USA

<sup>b</sup> CERN, PH-TH, CH-1211 Genève 23, Switzerland

<sup>c</sup> INR RAS, 60th October Anniversary pr. 7a, 117312 Moscow, Russia

<sup>d</sup> APC, Collège de France, 11 pl. Marcelin Berthelot, Paris 75005, France

We calculate the flux of “GZK-photons”, namely the flux of Ultra High Energy Cosmic Rays (UHECR) consisting of photons produced by extragalactic nucleons through the resonant photoproduction of pions, the so called GZK effect. We show that, for primary nucleons, the GZK photon fraction of the total UHECR flux is between  $10^{-4}$  and  $10^{-2}$  above  $10^{19}$  eV and up to the order of 0.1 above  $10^{20}$  eV. The GZK photon flux depends on the assumed UHECR spectrum, slope of the nucleon flux at the source, distribution of sources and intervening backgrounds. Detection of this photon flux would open the way for UHECR gamma-ray astronomy. Detection of a larger photon flux would imply the emission of photons at the source or new physics. We compare the photon fractions expected for GZK photons and the minimal predicted by Top-Down models. We find that the photon fraction above  $10^{19}$  eV is a crucial test for Top-Down models.

PACS numbers:

UCLA/04/TEP/17

### I. INTRODUCTION

The cosmic rays with energies beyond the Greisen-Zatsepin-Kuzmin (GZK) cutoff [1] at  $4 \times 10^{19}$  eV present a challenging outstanding puzzle in astroparticle physics and cosmology [2, 3]. Nucleons cannot be confined to our galaxy for energies above the “ankle”, i.e. above  $10^{18.5}$  eV. This and the absence of a correlation of arrival directions with the galactic plane indicate that, if nucleons are the primary particles of the ultra high energy cosmic rays (UHECR), these nucleons should be of extragalactic origin. However, nucleons with energies above  $5 \times 10^{19}$  eV could not reach Earth from a distance beyond 50 to 100 Mpc [4] because they scatter off the cosmic microwave background (CMB) photons with a resonant photoproduction of pions:  $p\gamma \rightarrow \Delta^* \rightarrow N\pi$ , where the pion carries away  $\sim 20\%$  of the original nucleon energy. The mean free path for this reaction is only 6 Mpc. Photons with comparable energy pair-produce electrons and positrons on the radio background and, likewise, cannot reach Earth from beyond 10 to 40 Mpc [5] (although the photon energy-attenuation length is uncertain, due to the uncertainties in the spectrum of the absorbing radio background). There only few known astrophysical sources within those distances that could produce such energetic particles, but they are not located along the arrival directions of observed cosmic rays.

Intervening sheets of large scale intense extra galactic magnetic fields (EGMF), with intensities  $B \sim 0.1 - 1 \times 10^{-6}$  G, could provide sufficient angular deflection for protons to explain the lack of observed sources in the directions of arrival of UHECR. However, recent realistic simulations of the expected large scale EGMF, show that strong deflections could only occur when particles cross

galaxy clusters. Except in the regions close to the Virgo, Perseus and Coma clusters the obtained magnetic fields are not larger than  $3 \times 10^{-11}$  G [6] and the deflections expected are not important (however see Ref. [7]).

Whether particles can be emitted with the necessary energies by astrophysical accelerators, such as active galactic nuclei, jets or extended lobes of radio galaxies, or even extended object such as colliding galaxies and clusters of galaxies, is still an open question. The size and possible magnetic and electric fields of these astrophysical sites make it plausible for them to produce UHECR at most up to energies of  $10^{21}$  eV. Larger emission energies would require a reconsideration of possible acceleration models or sites.

Heavy nuclei are an interesting possibility for UHECR primaries, since they could be produced at the sources with larger maximum energies (proportional to their charges) and would more easily be deflected by intervening magnetic fields. On the other hand, both AGASA and HiRes data favor a dominance of light hadrons, consisting with being all protons, in the composition of UHECR above  $10^{19}$  eV. However, we should keep in mind that the inferred composition is sensitive to the interaction models used. Assuming a proton plus iron composition, HiRes Stereo data show a constant or slowly changing composition of 80% protons and 20% iron nuclei between  $10^{18.0}$  eV and  $10^{19.4}$  eV. This is consistent with the change in composition from heavy to light in the  $10^{17}$  eV to  $10^{18}$  eV range found by HiRes Prototype [8]. HiRes monocular data show a 90% proton composition between  $10^{17.6}$  eV and  $10^{20}$  eV [9]. Similar results were found by AGASA, which produced bounds on the iron fraction (again assuming an iron plus proton composition) of 14 (+16, -14)% and 30 (+7, -6)% above  $10^{19.0}$  eV

and  $10^{19.25}$  eV respectively, and  $1\sigma$  upper bound of 66% above  $10^{19.5}$  eV [10].

In fact, a galactic component of the UHECR flux, which could be important up to energies  $10^{19}$  eV, should consist of heavy nuclei, given the lack of correlation with the galactic plane of events at this energy (outside the galactic plane, galactic protons would be deflected by a maximum of  $15\text{--}20^\circ$  at these energies [11]). For nuclei the dominant energy loss process is photodissociation through scattering with the infra-red background below  $10^{20}$  eV [12] and with the CMB above  $10^{20}$  eV, and pair creation on the CMB in a small energy interval around  $10^{20}$  eV (at energies for which the typical CMB photon energy in the rest frame of the nucleus is above threshold, i.e. above 1 MeV, but below the peak of the giant resonance, 10–20 MeV) [13]. The typical attenuation length in the energy range  $4 \times 10^{19}$  to  $1 \times 10^{20}$  eV changes from several  $10^3$  Mpc for iron and silicon to be comparable to that of nucleons for helium [13, 14]. At energies above  $1 \times 10^{20}$  eV, the attenuation length of heavy nuclei decreases and becomes less than 10 Mpc at about  $3 \times 10^{20}$  eV for iron,  $2 \times 10^{20}$  eV for silicon and  $1 \times 10^{20}$  eV for carbon (see for example Fig. 1 of Ref. [14]). In the realistically low EGMF of Ref. [6], most of the heavy nuclei with  $E > 10^{20}$  eV reaching us from more than 10 Mpc away with energies above those mentioned would disintegrate into protons with energy  $(1/A)$  of the original nucleus energy, where  $A$  is the atomic number (this is  $1/56$  of the original energy for iron nuclei). Note also that the same photodissociation processes can destroy heavy nuclei near their sources, if the intensity of the infrared background near the sources is large enough. One should not forget that all UHECR above  $10^{18}$  eV could be due to extragalactic protons [15].

The GZK cutoff at  $4 \times 10^{19}$  eV seems not to be present in the data of the AGASA ground array [2] but it appears in the data of the HiRes air fluorescence detector [3]. In any case, there are events above the GZK cutoff, even in the HiRes data set, and these remain unexplained since the local Universe ( $\sim 100$  Mpc) is devoid of strong candidate sources in the direction the events point to, and also of the large magnetic fields which could deflect the incoming particles significantly. Due to the limited statistics and different systematic errors of both experiments the discrepancy between them is not very significant. However, the presence or absence of the GZK cutoff remains an open question. This controversy will be solved conclusively by the Pierre Auger Observatory [16], a hybrid combination of charged particles detectors and fluorescence telescopes, perhaps within the next one or two years.

The analysis of the muon content in air showers has been used by AGASA to reject photon dominance in UHECR above  $10^{19}$  eV [10, 17]. Assuming a composition of protons plus photons, AGASA quotes upper limits for the photon ratio of 34%, 59% and 63% at  $10^{19}$  eV,

$10^{19.25}$  eV and  $10^{19.5}$  eV respectively at the 95% confidence level [10], and even above  $10^{20}$  eV they find no indication that the events they observe are mostly photons [17]. Also a reanalysis of horizontal showers at Haverah Park concluded that photons cannot constitute more than 50% of the UHECR above  $4 \times 10^{19}$  eV [18].

The GZK process produces pions. From the decay of  $\pi^\pm$  one obtains neutrinos. These “GZK neutrinos” have been extensively studied, from 1969 [19] onward (see for example [20, 21] and references therein), and constitute one of the main high energy signals expected in neutrino telescopes, such as ICECUBE [22] ANITA [23] and SALSA [24] or space based observatories such as EUSO [25] and OWL [26]. From the decay of  $\pi^0$  we obtain photons, “GZK photons”, with about 0.1 of the original proton energy, which have been known to be a subdominant component of the UHECR since the work of Wdowczyk *et al.* in the early 1970’s [27]. In 1990 it was suggested that if the extragalactic radio background and magnetic fields are small ( $B < 3 \times 10^{-11}$  G) GZK photons could dominate over protons and explain the super-GZK events [28]. The dependence of the GZK photon flux on extragalactic magnetic fields was later studied in Ref. [29]. The argument of Ref. [28] and its dependence on extragalactic magnetic fields was again discussed [30] in connection with the possible correlation of UHECR arrival directions with BL Lacertae objects [31]. However, to our knowledge, no complete study of the expected fluxes of GZK photons was done so far, including their dependence on the initial proton fluxes, distribution of proton sources and UHECR spectrum, besides intervening backgrounds.

With the advent of the Pierre Auger Observatory, we expect to have in the near future the high statistic data that may allow to study a subdominant component of UHECR consisting of photons. The GZK photons provide a complementary handle to GZK neutrinos and other signatures to try to determine the spectrum and composition of the UHECR. The flux of GZK photons is necessarily correlated with the flux of GZK neutrinos, although the former is affected by the radio background and EGMF values which do not affect the latter.

In this paper we show that if the UHECR are mostly protons, depending on the UHECR spectrum assumed, the slope of the proton flux, distribution of sources and intervening backgrounds, between  $10^{-4}$  and  $10^{-2}$  of the UHECR above  $10^{19}$  eV and between  $10^{-5}$  and 0.6 of the UHECR above  $10^{20}$  eV are GZK photons, the range being much higher for the AGASA spectrum than for the HiRes spectrum (see Fig. 17). Detection of these photons would open the way for UHECR photon astronomy.

Detection of a larger photon flux than expected for GZK photons would imply the emission of photons at the source or new physics. New physics is involved in Top-Down models, produced as an alternative to acceleration models to explain the origin of the highest energy

cosmic rays. All of the Top-Down models predict photon dominance at the highest energies. Here, we estimate the minimum photon fraction Top-Down models predict, not only assuming the AGASA spectrum which these models were originally proposed to explain, but also assuming the HiRes spectrum. We show that at high energy, close to  $10^{20}$  eV, the maximum expected flux of GZK photons is comparable to (for the AGASA spectrum) or much smaller than (for the HiRes spectrum) the minimum flux of photons predicted by Top-Down models which fit the AGASA or the HiRes data (see Fig. 17). We try to minimize the photon ratio predicted by Top-Down models by assuming that these models explain only the highest energy UHECR (if they do not explain even those events, the models are irrelevant for UHECR). We show that the photon ratio at energies close to  $10^{20}$  eV is a crucial test for Top-Down models, since it is always higher than about 0.5, independently of the UHECR spectrum assumed.

We also show that, surprisingly, in a limited energy range above  $10^{20}$  eV, GZK photons could become the dominant component of the UHECR (assuming that protons could be accelerated at the source to energies as large as  $10^{22}$  eV). This result allows us to fit the AGASA data with an original flux of only nucleons. This seems to contradict previous estimates of the GZK photon flux in which this flux is always subdominant, however one needs to take into account the assumed initial spectrum and intervening radio background and magnetic fields (for example in Ref. [20] an average EGMF of  $10^{-9}$  G is assumed, much larger than the fields found later in Ref. [6]).

In section II, we explain our calculations and show the dependence of the GZK photon flux on the assumed initial proton flux and intervening background parameters. In section II we only normalize the fluxes we show to one point of the AGASA or HiRes spectrum, but we do not fit these spectra (which we do in the following section). In section III, we estimate the maximum and minimum GZK photon fractions expected either with the AGASA spectrum or with the HiRes spectrum. In section IV we estimate the minimum photon fractions predicted by several by Top-Down models and compare them with the maximum GZK photon fraction we find in section III. We also include a comparison with experimental upper bounds on photon fractions.

## II. THE GZK PHOTON FLUX

We use a numerical code developed in Ref. [32] to compute the flux of GZK photons produced by an homogeneous distribution of sources emitting originally only protons. It calculates the propagation of protons and photons using the standard dominant processes, explained for example in Ref. [33]). For protons, it takes into

account single and multiple pion production, and  $e^\pm$  pair creation. For photons, it includes  $e^\pm$  pair production, inverse Compton scattering and double  $e^\pm$  pair production processes. For electrons and positrons, it takes into account Compton scattering, triple pair production and synchrotron energy loss on extra galactic magnetic fields (EGMF). The propagation of protons and photons is calculated self-consistently. Namely, secondary (and higher generation) particles arising in all reactions are propagated alongside with the primaries. UHE protons and photons lose their energy in interactions with the electro-magnetic background, which consist of CMB, radio, infra-red and optical components, as well as EGMF. Protons are sensitive essentially to the CMB only, while for photons all components of the electro-magnetic background are important. Notice that the radio background is not yet well known and that our conclusions depend strongly on the background assumed. We include three models for the radio background: the background based on estimates by Clark *et al.* [34] and the two models of Protheroe and Biermann [35], both predicting larger background than the first. To calculate the infra-red/optical background we used the same approach as in Ref. [36]. In any event, the infra-red/optical background is not important for the production and absorption of GZK photons at high energies. This background is important to transport the energy of secondary photons in the cascade process from the 0.1 - 100 TeV energy range to the 0.1-100 GeV energy range observed by EGRET. The resulting flux in the EGRET energy range is not sensitive to details of the infra-red/optical background models.

For the EGMF only the upper bound is established observationally,  $B \lesssim 10^{-9} (\text{Mpc}/l_c)^{1/2}$  G [37] (where  $l_c$  is the reversal scale of the magnetic field in comoving coordinates). It is believed that the magnetic fields in clusters can be generated from a primordial “seed” if the later has comoving magnitude  $B \sim 10^{-12}$  G [6, 38]. The evolution of EGMF together with the large scale structure of the Universe has been simulated recently by two groups using independent numerical procedures [6, 7]. Magnetic field strengths significantly larger than  $10^{-10}$  G were found only within large clusters of galaxies. In our simulations we vary the magnetic field strength in the range  $B = 10^{-12} - 10^{-9}$  G, assuming an unstructured field along the propagation path.

Notice that we assume that protons are produced at the source but the results at high energies would be identical if we had taken neutrons instead. The interactions of neutrons and protons with the intervening backgrounds are identical and when a neutron decays practically all of its energy goes to the final proton (while the electron and neutrino are produced with energies  $10^{17}$  eV or lower).

The resulting GZK photon flux depends on several astrophysical parameters. These parametrize the initial proton flux, the distribution of sources, the radio back-

ground and the EGMF. In this section, to explore the flux dependence on a given parameter, we fix all the other unknown parameters to the following values. For the radio background we take the lower estimate of Protheroe and Biermann [35], which is intermediate between the other two we consider. For the EGMF we take  $B = 10^{-11}$  G which is the average value found in Ref. [6]. For the source distribution, we take a uniform continuous distribution of sources with zero minimum distance to us (i.e. a minimum distance comparable to the interaction length). For the maximum energy of the injected protons we use  $E_{\max} = 10^{22}$  eV, which is considered already a generous upper limit for acceleration in astrophysical models [39].

With respect to cosmological parameters, we take the Hubble constant  $H = 70$  km s<sup>-1</sup> Mpc<sup>-1</sup>, a dark energy density (in units of the critical density)  $\Omega_{\Lambda} = 0.7$  and a dark matter density  $\Omega_m = 0.3$ . We assume the sources extend to a maximum redshift  $z_{\max} = 2$  (although any  $z_{\max} > 1$  gives the same results at the high energies we consider) and disregard a possible evolution of the sources with redshift.

### A. Dependence of the GZK photon flux on the initial proton spectrum

We parametrize the initial proton flux for any source with the following power law function,

$$F(E) = f \frac{1}{E^{\alpha}} \theta(E_{\max} - E). \quad (1)$$

The power law index  $\alpha$  and maximum energy  $E_{\max}$  are considered free parameters. The amplitude  $f$  is fixed by normalizing the final proton flux from all sources to the observed flux of UHECR, which we take to be either the AGASA flux or the HiRes flux.

We are implicitly assuming that the sources are astrophysical, since these are the only ones which could produce solely protons (or neutrons) as UHECR primaries. Astrophysical acceleration mechanisms often result in  $\alpha \gtrsim 2$  [40], however, harder spectra,  $\alpha \lesssim 1.5$  are also possible, see e.g. Ref. [41]. The resulting spectrum may differ from a power-law, it may even have a peak at high energies [42]. AGN cores could accelerate protons with induced electric fields, similarly to what happens in a linear accelerator. This mechanism would produce an almost monoenergetic proton flux, with energies as high as  $10^{20}$  eV or higher [43]. Here, we will consider the power law index to be in the range  $1 \leq \alpha \leq 2.7$ .

Fig. 1 shows the GZK photon flux for three values of the power law index in Eq. (1),  $\alpha = 1.5, 2$  and  $2.7$ . Dotted (solid) lines correspond to the resulting flux of protons (GZK photons) from all sources. A proton spectrum  $\sim 1/E^{2.7}$  does not require an extra contribution to fit the UHECR data, except at very low energies  $E < 10^{18}$  eV

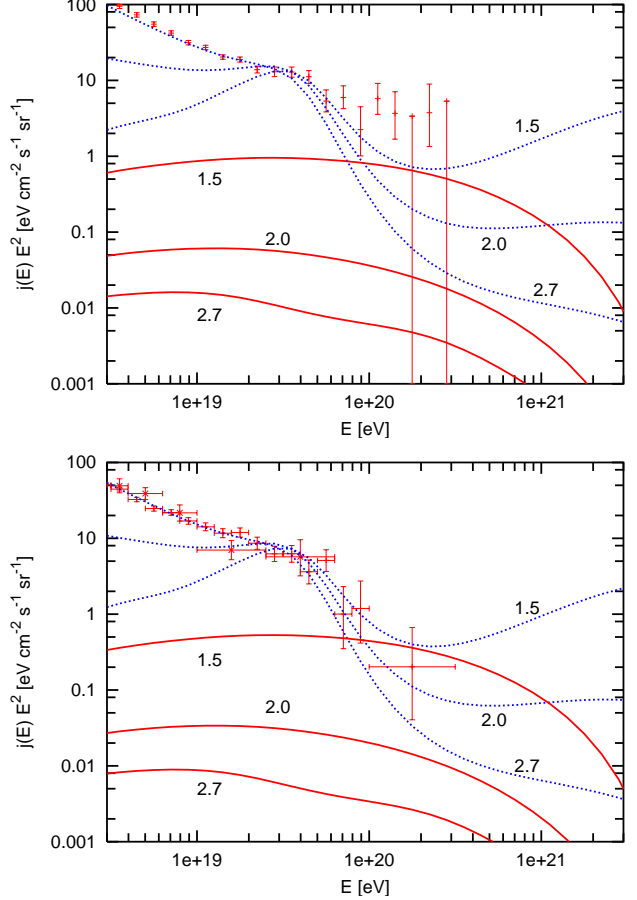


FIG. 1: UHECR proton flux (blue dotted lines) normalized to the AGASA data (upper panel) and HiRes data (lower panel) at  $3 \times 10^{19}$  eV and GZK photon flux (red solid lines) for three values of the power law index  $\alpha$  of the initial proton flux at the source:  $\alpha = 1.5, 2.0$  and  $2.7$  (from highest to lowest fluxes at high energy).

outside the range we study [44]. For  $\alpha \leq 2$  an extra low energy component (LEC) is required to fit the UHECR data at  $E < 10^{19}$  eV. The LEC may be a galactic contribution (for example of iron nuclei, to explain the lack of correlation of arrival directions with the galactic plane), which can be parametrized as power law with an exponential cutoff as in Eq.(2) below. In this case, the “ankle” is the energy where the extragalactic protons start to dominate over the LEC. The LEC could also be due to a population of extragalactic lower energy proton sources. This latter contribution can be parametrized again as in Eq. (1), but with parameters different than those of the extragalactic proton population which dominates above the GZK energy.

Notice that in this section we just normalize the total flux to a point of the AGASA or HiRes spectrum, but we do not fit these spectra, so we do not add a LEC, even if it would be needed. We do fit the UHECR spectrum in the next section.

As seen in Fig. 1, the flux of super-GZK protons and, consequently, the flux of the GZK photons they generate, depend strongly on the power law index of the initial proton flux: they are lower for large values of  $\alpha$ . In the most conservative case of a proton flux  $\sim 1/E^{2.7}$  the GZK photon flux at  $E = 10^{19}$  eV is as small as 0.03% and it increases to a few % at  $E = 2 \times 10^{20}$  eV. This means that even with the final statistics of Auger it might be difficult to detect the GZK photons in this case. On the other hand, in the optimistic case of an injection spectrum  $\sim 1/E^{1.5}$ , the GZK photons can contribute as much as 1-3% at  $E = 10^{19}$  eV and 50% or more at  $E = 10^{20}$  eV.

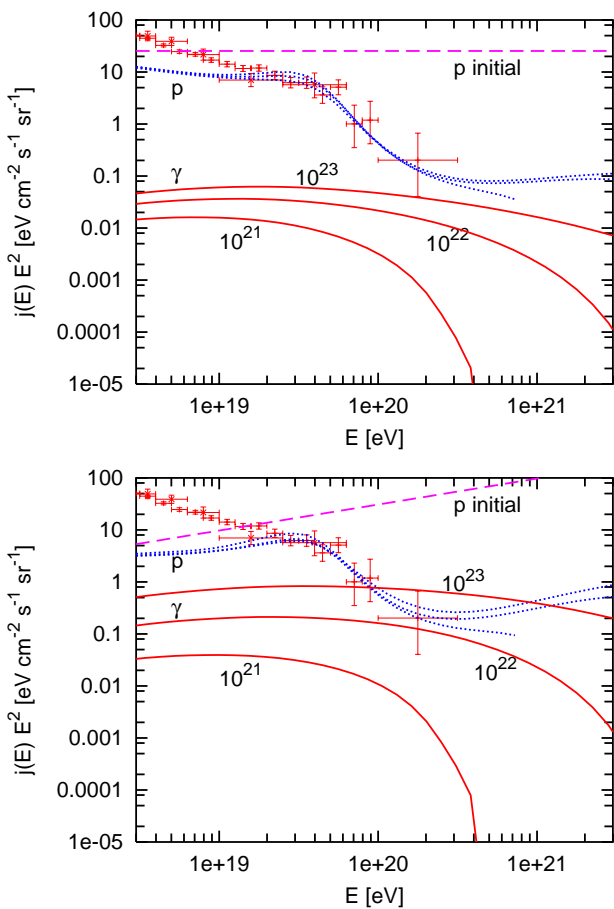


FIG. 2: UHECR proton flux (dotted lines) normalized to the HiRes data at about  $3 \times 10^{19}$  eV and GZK photon flux (solid lines) for three values of the maximal energy of the initial proton spectrum:  $E_{\max} = 10^{23}$  eV,  $10^{22}$  eV and  $10^{21}$  eV (from highest to lowest fluxes at high energy). The initial proton flux is (a)  $\sim 1/E^2$  (upper panel) and (b)  $\sim 1/E^{1.5}$  (lower panel)

Let us note here, that most of the energy produced in the form of GZK photons cascades down in energy to below the pair production threshold for photons on the CMB. For  $\alpha < 2$  the diffuse extragalactic gamma-ray flux measured by EGRET [45] at GeV energies imposes

a constraint on the GZK photon flux at high energies, which we have taken into account.

The dependence of the GZK photon flux on the maximum energy  $E_{\max}$  of the initial proton flux (see Eq. (1)) is shown in Fig. 2, for  $E_{\max} = 10^{21}$  eV,  $10^{22}$  eV and  $10^{23}$  eV. We do not show here the case of  $\alpha = 2.7$  because for such a steeply falling proton flux the GZK photon flux practically does not depend on  $E_{\max}$ . Fig. 2a shows the case of  $\alpha = 2$  and Fig. 2b that of  $\alpha = 1.5$ . These figures clearly show that the dependence on  $E_{\max}$  is more significant for smaller values of the power law index  $\alpha$ . Note that not only the photon flux, but also the final UHECR proton flux above the GZK cutoff depends strongly on  $E_{\max}$ .

For relatively small values of the maximal energy, such as  $E_{\max} = 10^{21}$  eV, the GZK photon flux is very small for any power law index  $\alpha$  (see the lowest curves in Fig. 2a and Fig. 2b). For larger values of the maximal energy, such as  $E_{\max} = 10^{22}$  eV and  $E_{\max} = 10^{23}$  eV, the GZK photon flux increases considerably for  $\alpha \leq 2$ .

## B. Dependence of the GZK photon flux on the minimal distance to the sources

Quite often in the literature the minimal distance to the sources is taken to be negligible (i.e. comparable to the interaction length). This is one of the cases we consider as well. However we take also 50 Mpc, as inferred from the small-scale clustering of events seen in the AGASA data [46], and 100 Mpc, to show how the fluxes diminish with this assumption (what proves that most photons come from smaller distances). Contrary to AGASA, HiRes does not see a clustering component in its own data [47]. The combined dataset shows that clustering still exists, but it is not as significant as in the data of AGASA alone [48]. Note, that the non-observation of clustering in the HiRes stereo data does not contradict the result of AGASA, because of the small number of events in the sample [49].

Assuming proton primaries and a small EGMF (following Ref. [6]), it is possible to infer the density of the sources [49, 50] from the clustering component of UHECR. AGASA data alone suggest a source density of  $2 \times 10^{-5}$  Mpc<sup>-3</sup>, which makes plausible the existence of one source within 50 Mpc of us. However, the HiRes negative result on clustering requires a larger density of sources and, as a result, a smaller distance to the nearest one of them. Larger values of the EGMF (as found in Ref. [7]) and/or some fraction of iron in the UHECR have the effect of reducing the required number of sources and, consequently, increasing the expected distance to the nearest one.

Fig. 3 shows the dependence of the UHECR proton and GZK photon fluxes on the assumed minimal distance to sources for an initial proton flux  $\sim 1/E^2$  in Fig. 3a and  $\sim 1/E^{1.5}$  in Fig. 3b. The highest, intermediate and low-

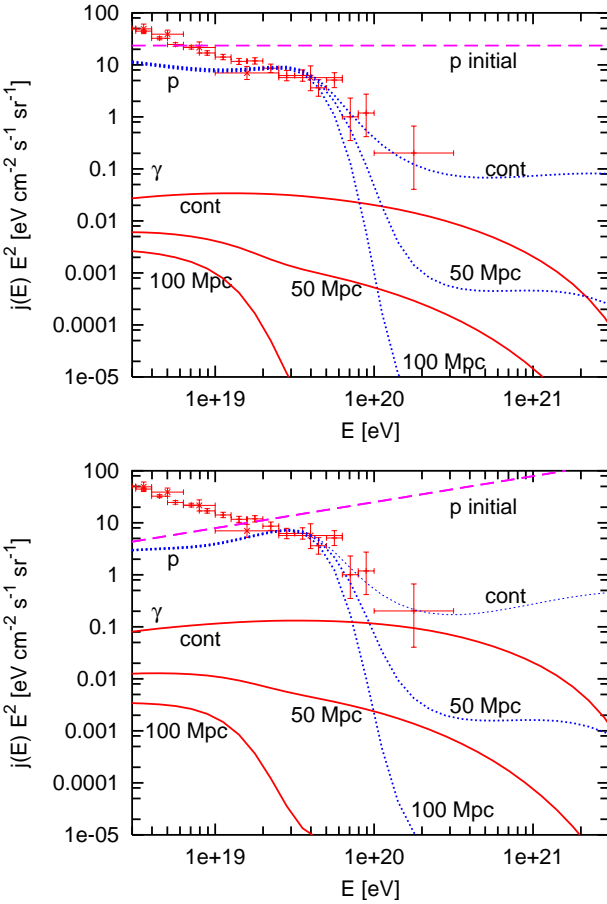


FIG. 3: UHECR proton flux (dotted lines) normalized to the HiRes data at  $4 \times 10^{19}$  eV and GZK photon flux (solid lines) for three values of the minimal distance to the sources: 0, 50 Mpc and 100 Mpc, (from highest to lowest fluxes at high energy) for an initial proton flux (a)  $1/E^2$  (upper panel) and (b)  $1/E^{1.5}$  (lower panel).

est fluxes correspond to a minimal distance of 0 (labeled cont. for continuous), 50 and 100 Mpc, respectively. Notice that in all the examples presented in Fig. 3 the protons dominate the flux (i.e. the total flux is practically the proton flux). Only the highest proton fluxes shown in Fig. 3 (with negligible minimal distance) fit well the HiRes data. The intermediate and lowest proton fluxes have a sharp cutoff and do not fit the HiRes data any longer. We clearly see in the figures that most of the GZK photons with energies  $E > 10^{19}$  eV should come from nearby sources within 100 Mpc (see the impressive reduction in flux if we only take sources more than 100 Mpc away).

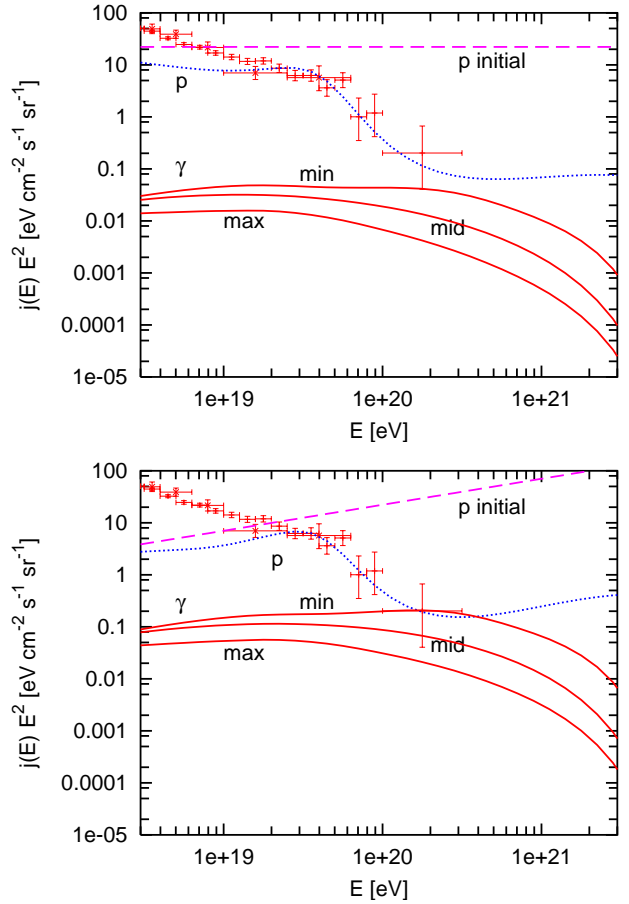


FIG. 4: UHECR proton flux (dotted lines) normalized to the HiRes data at  $4 \times 10^{19}$  eV and GZK photon flux (solid lines) for the three estimates of radio background considered in this paper. The initial proton spectrum in (a) is  $\sim 1/E^2$  (upper panel) and in (b) is  $\sim 1/E^{1.5}$  (lower panel).

### C. Dependence of the GZK photon flux on the radio background

The main source of energy loss of photons with  $E > 10^{19}$  eV is pair production on the radio background (while at lower energies pair production on the CMB is more important). Fig. 4 shows GZK photon fluxes for the three different estimates of the radio background we consider: the minimal background, of Clark et al. [34], and the two estimates of Protheroe and Biermann [35], both larger than the first one. In Fig. 4a the injected proton spectrum  $\sim 1/E^2$  and in Fig. 4b it is  $\sim 1/E^{1.5}$ . These figures show that (for the EGMF assumed,  $B = 10^{-11}$  G as mentioned above) the GZK photon flux depends only mildly on the radio background at energies below  $E < 10^{20}$  eV, where we find a factor 2-3 of difference between the highest flux (with the lowest radio background from Ref. [34]) and the lowest flux (with the highest background of Ref. [35]). However, at energies above  $E > 10^{20}$  eV, the differences increase, reaching one order of magnitude or

more. This behavior is due to the different shapes of the assumed radio spectra. As we see next, larger EGMF,  $B > 10^{-10}$  G, increase the GZK photon absorption considerably at  $E < 10^{20}$  eV, but not close to  $E \simeq 10^{20}$  eV and above.

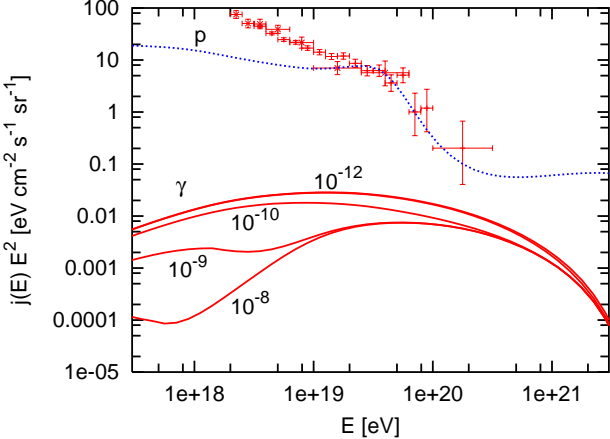


FIG. 5: UHECR proton flux (dotted lines) normalized to the HiRes data at  $3 \times 10^{19}$  eV and GZK photon flux (solid lines) for four values of the average EGMF,  $10^{-12}$  G,  $10^{-10}$  G,  $10^{-9}$  G and  $10^{-8}$  G (from highest to lowest fluxes), for a proton flux  $\sim 1/E^2$ .

#### D. Dependence of the GZK photon flux on EGMF

The spacial structure, amplitude and correlation length of the EGMF outside clusters of galaxies are unknown. The existing models of the EGMF attempt to evolve these fields together with the large scale structure of the Universe, starting from certain (primordial) seed values. In these models, the EGMF in the voids are close to the comoving value of the primordial field, while the EGMF in clusters of galaxies and filaments are amplified. Constrained simulations of the “local” Universe (within 100 Mpc from Earth) [6], in which the magnetic field is normalized to the values observed within clusters, yield an average  $B_{\text{EGMF}} = (10^{-11} - 10^{-12})$  G in voids. Fig. 5 shows that for  $B_{\text{EGMF}} < 10^{-10}$  G, the resulting GZK photon flux changes very little with  $B$ , but it decreases considerably at low energies for  $B_{\text{EGMF}} \gtrsim 10^{-9}$  G. In Fig. 5 an initial proton flux  $\sim 1/E^2$  was assumed and sources were integrated from zero distance. Assuming a minimum distance of 50 Mpc to the nearest sources (case not shown in the figures), the GZK photon fluxes differ at most by a factor of 3 when the EGMF magnitude is varied in the range  $B < 10^{-10}$  G.

Fig. 5 is the only place in this paper where we used  $B_{\text{EGMF}} = 10^{-8}$  G, and this is just to show how the photon flux is affected by large  $B$  fields. For EGMF  $\sim 10^{-8}$  G or larger, the photon energy is lost into

synchrotron radiation as soon as the UHE photon pair produces, even for energies  $E < 10^{19}$  eV. Thus the shape of the spectrum follows the energy dependence of the photon pair production interaction length (which is dominated by the interaction with the CMB below  $10^{19}$  eV and with the radio background above this energy). For smaller magnetic field strengths, the length of synchrotron energy loss increases and, at low energies, several steps of pair production and inverse Compton decay happen. For large enough energies, the synchrotron radiation length is smaller than the interaction length for all the EGMF values considered (i.e. even as small as  $B \geq 10^{-12}$  G), so the photon energy is lost into synchrotron radiation as soon the photon pair produces. Thus, only the photons which do not interact with the radio background can reach us and the spectra for all values of the EGMF converge.

Our results in Fig. 5 for  $B_{\text{EGMF}} \leq 10^{-9}$  G are similar to those in Fig. 3 of Ref. [29]. In particular, both figures show that the GZK flux does not depend strongly on the magnetic field for  $B_{\text{EGMF}} < 10^{-10}$  G, and that for larger fields there is a suppression of the photon flux at energies  $E < 10^{19}$  eV (due to pair production on the CMB followed by synchrotron energy loss).

#### E. Summary of the GZK photon flux dependence on different parameters

Figs. 4 and 5 show that given a particular UHECR proton flux the uncertainty in the resulting GZK photon flux due to our ignorance of the intervening backgrounds (minimum to maximum estimates of the radio background and EGMF from  $10^{-11}$  G, which is equivalent to zero, to  $10^{-9}$  G) is within about one order of magnitude.

Figs. 1 to 3 show much larger changes in the GZK photon flux when the parameters defining the UHECR proton flux, i.e. the power law index  $\alpha$ , maximum energy  $E_{\text{max}}$ , and minimal distance to the sources, are varied. However, once the particular UHECR spectrum is fixed, these uncertainties due to the extragalactic proton model decrease and become comparable with those due to our ignorance of the intervening background. In the next section, Figs. 8 and 9 show that a particular proton dominated observed flux, the HiRes spectrum in this case, can be fitted with very different extragalactic proton fluxes, whose corresponding GZK photon fluxes differ by about one order of magnitude, for a given fixed background. In fact, the difference between the two photon lines in Fig. 8 shows the uncertainty in the GZK photon flux due to intervening background (about one order of magnitude), given a particular extragalactic proton flux, while the difference between the lower photon line of Fig. 8 and the lower photon line of Fig. 9 (both computed with the same background, i.e. maximum radio background and

EGMF  $B = 10^{-9}$  G) shows the uncertainty due to the UHECR proton flux (which is one order of magnitude too).

This means that placing an upper limit on the GZK photon flux, or measuring it, provides complementary information to that contained in the UHECR proton flux itself. However, extracting information on the extragalactic nucleon flux from the GZK photons would require to have independent information on the extragalactic magnetic fields and radio background, vice versa.

### III. RESULTS: POSSIBLE SCENARIOS WITH GZK PHOTONS

We show in Sect. II that if the UHECR above  $10^{19}$  eV are mostly protons (or neutrons), depending on the slope of the proton flux, the distribution of sources and the intervening backgrounds, between  $10^{-5}$  and  $10^{-2}$  of the UHECR above  $10^{19}$  eV are photons. Much larger photon fractions are predicted at  $10^{20}$  eV in some cases.

The largest GZK photon fractions in UHECR happen for small values of  $\alpha$ , large values of  $E_{\max}$ , small minimal distance to the sources (which is compatible with a small frequency of clustering of the events) and small intervening backgrounds. In the most favorable cases for a large photon flux, GZK photons could dominate the UHECR flux in an energy range above  $10^{20}$  eV. As we show below, this allows us to fit the AGASA data, at the expense of assuming that the initial protons could have a hard spectrum  $\sim 1/E$  and be accelerated to energies as high as  $10^{22}$  eV. In this extreme case, the AGASA data (as shown in subsection III-A below) can be explained without any new physics, except in what the mechanism of acceleration of the initial protons is concerned. We also fit the HiRes spectrum (in III-B below). With the HiRes spectrum the GZK photons are always subdominant and can be neglected for the fit. In both cases, AGASA or HiRes data, we evaluate the minimum and maximum GZK photon fractions expected with each spectrum of UHECR.

We make a one-parameter  $\chi^2$  fit to the assumed total spectrum, obtained by summing up the contributions of protons, GZK photons and a low energy component (LEC) when needed.

In this section we parametrize the LEC with

$$F_{\text{LEC}} \sim E^{-\beta} \exp(-E/E_{\text{cut}}). \quad (2)$$

and we fit the amplitude to the lowest energy bin in the figures. We choose the parameter  $\beta = 2.7 - 2.8$  to fit the low energy spectral points, and the parameter  $E_{\text{cut}}$  so that the minimum  $\chi^2$  value per degree of freedom of the fit is smaller than one.

We use the 18 highest energy data bins of AGASA and the 16 highest energy data bins of HiRes-1 monocular data. We also separately check the  $\chi^2$  for the AGASA events above the GZK cutoff, i.e. for the 3 highest energy

AGASA data bins, with  $E > 10^{20}$  eV. We do this to exclude models which do not fit well the highest energy events but whose minimum  $\chi^2$  considering all the 18 bins could be good due to the LEC assumed. Additionally, we check that the number of events predicted above the end point of the AGASA spectrum (the energy above which AGASA has observed no events), i.e. at  $E > 2.5 \times 10^{20}$  eV, is not larger than 4 (predicting 4 events and observing none has a very small Poisson probability of 1.8%). The number of events we predict above the end point of the HiRes spectrum, at  $E > 3.2 \times 10^{20}$  eV, is always much smaller than 4.

#### A. GZK photons with the AGASA spectrum

In this subsection, we will discuss fits to the AGASA data with extragalactic protons, their secondary GZK photons and a LEC as in Eq. (2) when needed. Unless we mention otherwise, here we take a zero (i.e. comparable with the interaction length) minimum distance to the sources.

The fits to the AGASA spectrum at high energy with a proton dominated flux are very poor. As shown in Fig. 1, for  $\alpha < 2.7$  a low energy component (LEC) which we parametrize as in Eq. (2), possibly consisting of galactic or extragalactic Fe and protons, is necessary to fit the data. It is well known that with extragalactic protons plus a LEC one can fit the AGASA data below the GZK cutoff, at energies  $3 \times 10^{18}$  eV  $< E < 10^{20}$  eV. In fact, we tried power law indexes  $\alpha = 2.7, 2, 1.5, 1$  and we obtained fits with minimum  $\chi^2 = 36, 17.7, 14, 14$  for 15 degrees of freedom, respectively. The first fit (with  $\alpha = 2.7$ , which does not require a LEC) is bad, but the others (which do require a LEC) are good. Even the first fit could be improved to a minimum  $\chi^2 = 18$  by changing the power index slightly to  $\alpha = 2.6$  and increasing the number of sources in the early universe as  $(1+z)^3$ . However, the same proton fluxes fit the AGASA data at  $E > 10^{20}$  eV very poorly. We found minimum  $\chi^2 = 12, 12, 9.8, 7.8$  for 3 degrees of freedom, respectively. The reason for these bad fits is that for  $\alpha \geq 2$  the proton flux at super-GZK energies is very small, and even for  $\alpha < 2$  it is still not enough.

These fits can be improved by adding a large component of GZK photons. We try to maximize the GZK photon flux by reducing the radio background and EGMF, and increasing the maximum proton energy in Eq. (1) up to  $E_{\max} = 10^{22}$  eV.

In Figs. 6 and 7 we show (a) the differential spectra, of each component (i.e. extragalactic  $p$ , LEC and GZK  $\gamma$ ) and total (upper panels), and (b) the integrated flux fractions of different components in percentage of the total predicted flux above the energy  $E$  (lower panels). The extragalactic protons have here an initial spectrum  $\sim 1/E$ , with maximum energy  $E_{\max} = 10^{22}$  eV (see Eq. (1)).

The particular LEC shown has parameters  $\beta = 2.7$  and cutoff energy  $E_{\text{cut}} = 10^{19}$  eV (see Eq. (2)). In both Figs. 6 and 7 the EGMF is  $B = 10^{-11}$  G. The only difference between both figures is the radio background: we took the lowest one for Fig. 6 and the intermediate one for Fig. 7. This is the only change we can impose between the maximum and the minimum GZK photon flux while not reducing the goodness of fit to the AGASA data to unacceptable levels.

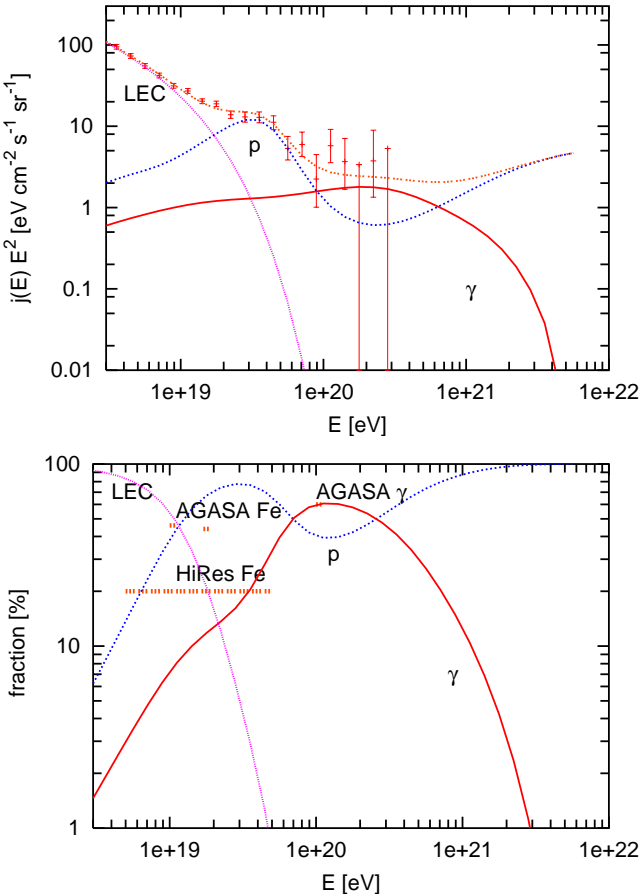


FIG. 6: Example of a fit to the AGASA data with extragalactic protons, the GZK photons they produce and a low energy component (LEC) at  $E < 10^{19}$  eV. (a) differential spectra (upper panel) and (b) fraction in percentage of the integrated flux above the energy  $E$  of every component (lower panel). Here we try to **maximize** the photon component thus we take an extragalactic proton spectrum  $\sim 1/E$  with maximum energy  $E_{\text{max}} = 10^{22}$  eV,  $B_{\text{EGMF}} = 10^{-11}$  G and the minimum radio background. Also shown in (b) are the  $2\sigma$  AGASA upper bounds on the Fe fraction above  $10^{19.0}$  eV and  $10^{19.25}$  eV [10], the HiRes limits on Fe component [9] and the bound on the photon fraction obtained with AGASA data at  $10^{20}$  eV [51].

The fit to the super-GZK AGASA events in Fig. 6a is now perfect, due to the GZK photons: it has a minimum  $\chi^2 = 2.6$  for 3 degrees of freedom and at  $E > 10^{20}$  eV there are 11.5 events (6.8 photons and 4.5 protons) where

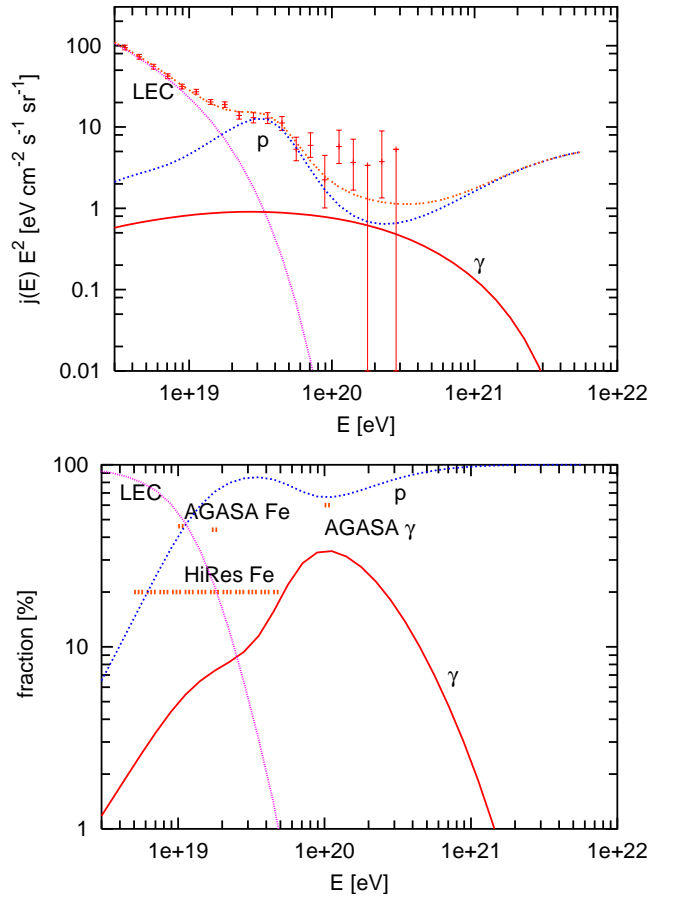


FIG. 7: Same as Fig. 6 but with reduced GZK photon flux due to assuming the intermediate extragalactic radio background (instead of the lowest). Here we try to **minimize** the photon component while still providing a good fit to the AGASA data.

AGASA has observed 11. The spectrum predicts 4 events (2 photons and 2 protons) at energies above  $2.5 \times 10^{20}$  eV, where AGASA has seen none, which we take as acceptable (the probability is small, 1.8%). Larger  $E_{\text{max}}$  or lower  $\alpha$  values would lead to predict even more events where AGASA has seen none and would therefore not fit well the AGASA spectrum any longer.

The fit to the super-GZK AGASA events in Fig. 7a, where we try to lower the GZK flux, is not as good as that in Fig. 6a: it has a minimum  $\chi^2 = 5.5$  for 3 degrees of freedom and at  $E > 10^{20}$  eV there are 7 events (2.5 photons and 4.5 protons). But, this fit is better than that in Fig. 6a above the end-point of the AGASA spectrum: it predict only 2.7 events above the highest energy AGASA point, which has a 6.7% Poisson probability.

As we see, a good fit to the AGASA data at  $E > 10^{20}$  eV with GZK photons is strongly restricted by the total number of events on one side and by the number of events above the end-point of the AGASA spectrum on the other. Thus, Figs. 6-7 provide an estimate of the

maximum and minimum GZK photon flux which fit the AGASA data.

Notice in Fig. 6b that with the maximum GZK photon flux prediction, the photon ratio increases from about 7 % at  $10^{19}$  eV to more than 50 % above  $10^{20}$  eV, and that the total differential flux is dominated by GZK photons at energies between 1 and  $7 \times 10^{20}$  eV. This large GZK photon flux is possible only under the extreme conditions chosen here. A larger radio background, or a smaller maximum proton energy quickly diminish the GZK photon flux, as Fig. 7 demonstrates.

The EGRET bound on the photon energy which cascades down to the GeV energies has been taken into account. We found that the flux predicted is about one order of magnitude below the level measured by EGRET.

The  $2\sigma$  AGASA upper bounds on the Fe fraction in the integrated fluxes, of 46% and 44% above  $10^{19.0}$  eV and  $10^{19.25}$  eV respectively [10] are shown in Fig. 6b and Fig. 7b. The LEC could respect these bounds (so that the LEC could consist entirely of galactic Fe), if we assumed a somewhat softer proton spectrum than we choose for Figs. 6 and 7, possibly with  $\alpha \gtrsim 1.5$ . With our choice, the extragalactic proton spectrum is a bit too low at energies below the GZK energy and, consequently, the LEC is too large. The lower HiRes limit on a possible Fe low energy component [9], rejects entirely a LEC consisting mostly of iron. In this case the LEC should consist mostly of extragalactic protons with a soft spectrum  $\sim 1/E^{2.7}$  and a small maximum energy  $E_{\max} \ll 10^{20}$  eV which should come from a different class of UHECR sources (than those which produce the super-GZK UHECR).

Also shown in Fig. 6b and Fig. 7b is the bound on the photon fraction obtained with AGASA data at  $10^{20}$  eV [51], which is saturated by the photon flux in Fig. 6.

### B. GZK photons with the HiRes spectrum

To estimate the possible range of photon fractions compatible with the HiRes spectrum we will here present two fits to the HiRes data, one maximizing and one minimizing the GZK photon flux. These fits are presented in Figs. 8 and 9 respectively.

Figs. 8 show (a) the differential spectra of each component (i.e. extragalactic protons, LEC and GZK photons) and total and (b) the integrated flux fractions of different components with respect to the total predicted flux shown in Fig. 8a. In order to maximize the flux of GZK photons we need a relatively hard proton spectrum, thus a LEC is needed to fit the data at energies  $E < 10^{19}$  eV. The particular LEC shown has parameters  $\beta = 2.7$  and cutoff energy  $E_{\text{cut}} = 2 \times 10^{19}$  eV (see Eq. (2)). Here we assume an extragalactic proton spectrum  $\sim 1/E$  with maximum energy  $E_{\max} = 10^{21}$  eV, to maximize the number of super-GZK protons, and to minimize the photon absorp-

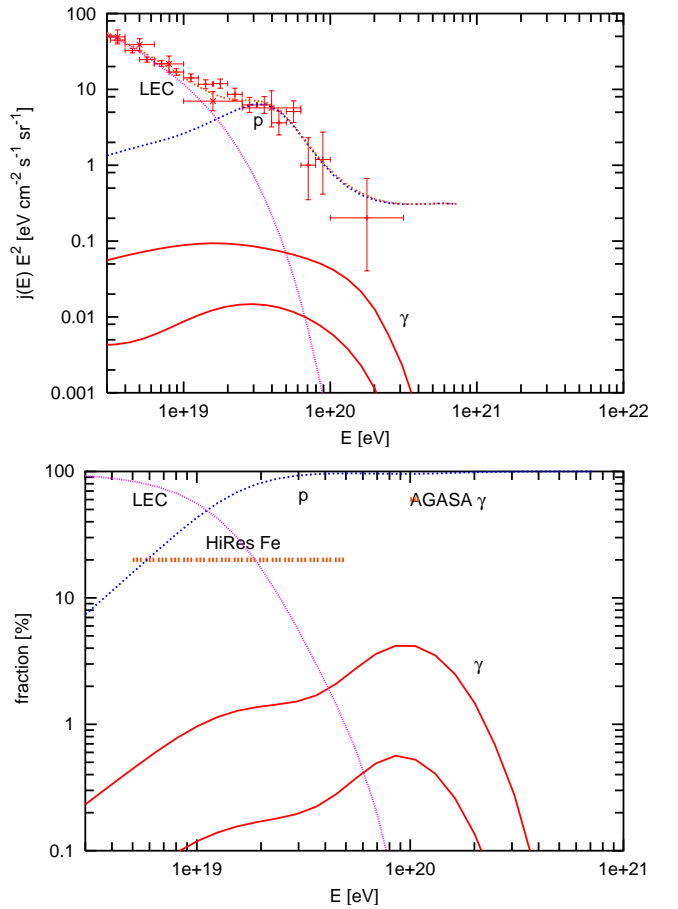


FIG. 8: Example of a fit to the HiRes data with extragalactic protons, the GZK photons they produce and a low energy component (LEC) at  $E < 10^{19}$  eV. (a) Differential spectra (upper panel) and (b) fraction in percentage of the total integrated predicted flux above the energy  $E$  of every component (lower panel). Here we try to **maximize** the photon component thus we take an extragalactic proton spectrum  $\sim 1/E$  with maximum energy  $E_{\max} = 10^{21}$  eV, minimum radio background and  $B_{\text{EGMF}} = 10^{-11}$  G for the higher photon curve (maximum radio background and  $B_{\text{EGMF}} = 10^{-9}$  G for the lower photon curve). Also shown in (b) are the HiRes limits on a possible Fe low energy component [9] and the bound on the photon fraction obtained with AGASA data at  $10^{20}$  eV [51].

tion by the intervening medium, we assume the minimum radio background and  $B_{\text{EGMF}} = 10^{-11}$  G. This results in the higher photon curve in the figures. The lower photon curve shows how much the photon flux decreases if we keep the same proton flux and change the intervening background from minimum to maximum, i.e. if we use  $B_{\text{EGMF}} = 10^{-9}$  G and maximum radio background. The change is about an order of magnitude.

The total flux shown in Fig. 8a is dominated by protons and is insensitive to the GZK photon contribution. With this flux only one event (a proton event) is predicted above  $1 \times 10^{20}$  eV.

Also shown in Fig. 8b are the HiRes limits on a possible

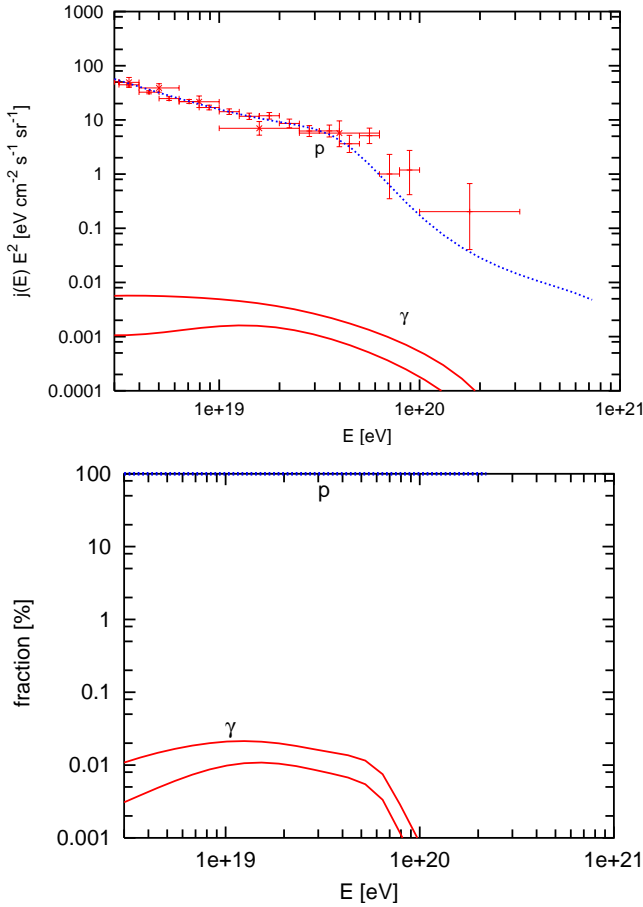


FIG. 9: Example of a fit to the HiRes data with extragalactic protons, the GZK photons they produce and a low energy component (LEC) at  $E < 10^{19}$  eV. (a) Differential spectra (upper panel) and (b) fraction in percentage of the integrated total predicted flux above the energy  $E$  of every component (lower panel). Here we try to **minimize** the photon component thus we take an extragalactic proton spectrum  $\sim 1/E^{2.7}$  with maximum energy  $E_{\max} = 3 \times 10^{20}$  eV, maximum radio background and  $B_{\text{EGMF}} = 10^{-9}$  G for the lower photon curve ( $B_{\text{EGMF}} = 10^{-11}$  G and intermediate radio flux for the higher photon curve). The total flux is dominated by nucleons at all energies and is lower than the HiRes data at high energies. This is about the best fit that can be done to the HiRes spectrum with a proton dominated flux. Also shown in (b) are the HiRes limits on a possible LEC Fe component [9] and the bound on the photon fraction obtained with AGASA data at  $10^{20}$  eV [51].

LEC Fe component [9] and the bound on the photon fraction obtained with AGASA data at  $10^{20}$  eV [51].

In Fig. 9 we fit the HiRes data with a conservative model with a soft extragalactic proton spectrum, which does not require a low energy component. Thus, the power law index of the required proton spectrum is fixed by the observed UHECR at energies below  $10^{19}$  eV, where the spectrum is  $\sim 1/E^{2.7}$ . This model has practically no freedom in the choice of the proton flux power law index  $\alpha$ , although this could be slightly varied in the range

$\alpha = 2.4 - 2.7$  by changing the redshift dependence of the distribution of sources. For Fig. 9 we conservatively choose  $\alpha = 2.7$  and the smallest cutoff energy which provides a good fit, which is  $E_{\max} = 3 \times 10^{20}$  eV. We assume zero minimal distance to the sources (larger values do not provide a good fit at high energies), and, to maximize the absorption of photons, the maximum radio background and  $B_{\text{EGMF}} = 10^{-9}$  G for the lower photon curve. We also give the result for  $B_{\text{EGMF}} = 10^{-11}$  G and intermediate radio background (higher photon curve) to show how the photon flux increases with a less absorbing intervening background. The total flux is insensitive to the GZK photon contribution.

The difference between the lower photon line of Fig. 8 and the lower photon line of Fig. 9 (both computed with the same background) shows the uncertainty due to the UHECR proton flux (which is one order of magnitude too) for models that fit the HiRes spectrum.

Also shown in Fig. 9b are the HiRes limits on a possible LEC Fe component [9] and the bound on the photon fraction obtained with AGASA data at  $10^{20}$  eV [51].

We see in Fig. 9b that in this case, in which we try to minimize the GZK photons, these could contribute only  $1 - 2 \times 10^{-4}$  at  $10^{19}$  eV, and  $1 - 2 \times 10^{-5}$  at  $10^{20}$  eV, of the total integrated flux. These levels of photon fraction are out of reach for the present generation of experiments. At best Auger would detect a few GZK photons in several years of observations, while HiRes would only obtain upper limits on the number of photons at all energies.

#### IV. DISCUSSION: COMPARISON OF GZK PHOTONS, MINIMUM TOP-DOWN PHOTON PREDICTIONS AND EXPERIMENTAL BOUNDS

In this section we discuss the present experimental bounds on and theoretical predictions for UHECR photons, and discuss the implications of a possible future photon detection or future experimental upper limits on the photon fraction.

We start by comparing the minimal amount of photons predicted by Top-Down models of UHECR with the expected range of GZK photons discussed in Sect. III. We show that, at high energies, close to  $10^{20}$  eV, the maximum expected flux of GZK photons is comparable to (for the AGASA spectrum) or much smaller than (for the HiRes spectrum) the minimum flux of photons predicted by Top-Down models which fit the AGASA or the HiRes data. Thus, detection of a larger photon flux than expected for GZK photons, at those energies, would point to a Top-Down model (or to the emission of a large flux of photons at the sources). The estimate of the minimum photon ratio predicted by Top-Down models is also essential when applying to these models already existing and possible future upper bounds on the fraction of photons in UHECR.

Let us recall that Top-Down models were introduced as an alternative to acceleration models to explain the highest energy cosmic rays, which the latter models have difficulty explaining. The spectra of the UHECR produced in Top-Down models are determined by the elementary particle physics of Z-boson decays and of QCD fragmentation, which predict photon domination of the spectrum at high energies.

In order to **minimize** the photon fraction predicted by Top-Down models while fitting the UHECR spectrum, we ask Top-Down models to explain only the highest energy events, those close to  $10^{20}$  eV while invoking a more conventional Bottom-Up extragalactic component (which we assume consists of nucleons) to dominate the flux at energies just below. This is an unnatural possibility which would require two completely independent mechanisms to provide UHECR at comparable levels. We consider it only because it provides the minimum amount of Top-Down photons. We will present here fits to the AGASA and HiRes data following this strategy to minimize the predicted photons for three Top-Down models: Z-bursts, topological defects (necklaces) and super heavy dark matter particles (SHDM).

### A. Z-bursts

In the Z-burst model [52] ultra-high energy (UHE) neutrinos coming from remote sources annihilate at the Z-resonance with relic background neutrinos. The Z bosons then decay, producing secondary protons, neutrinos and photons. The Z-resonance, which acts as a new cutoff, occurs when the energy of the incoming  $\nu$  is  $E_{res} = M_Z^2/2 m_\nu = 4 \times 10^{21}$  eV/(eV/ $m_\nu$ )

So far Z-burst models have been studied mostly to explain the AGASA spectrum (however, see Ref. [53]). Many problems have been found, which are alleviated if one assumes the HiRes spectrum. One of them is that practically no photons should be produced at the source together with the UHECR neutrinos, otherwise too many low energy photons in the EGRET region are predicted. For example, with sources emitting equal power in neutrinos and photons, the EGRET bound [45] on the diffused GeV-  $\gamma$  ray background is violated by two orders of magnitude (see Fig. 3 of Ref. [54]), when the AGASA spectrum is considered. Also bounds by the GLUE [55] and FORTE [56] experiments on the primary neutrino flux, as well as the non-observation of UHECR events at energies above  $2.5 \times 10^{20}$  eV by the AGASA Collaboration imply a lower bound  $\sim 0.3$  eV on the relic neutrino mass [21, 53, 57]. Since this mass exceeds the square root of mass-squared differences inferred from oscillation physics, the bound in fact applies to all three neutrino masses. Together with the upper bound provided by CMB anisotropy and large-scale structure observations, this bound leaves only a small interval for

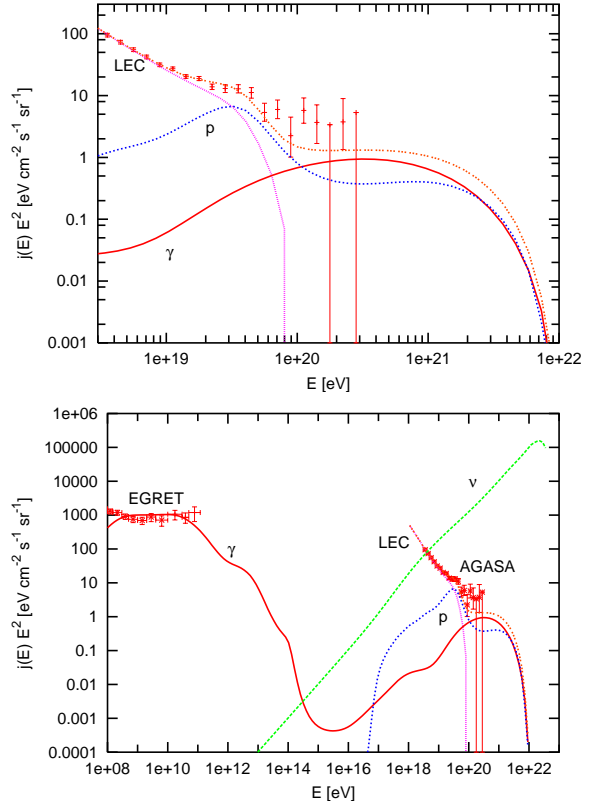


FIG. 10: Example of a fit to the AGASA data with a LEC plus a flux of protons and photons produced by Z-bursts (a) showing the highest energies and (b) showing also the EGRET energy region. LEC due to protons from astrophysical sources. Also shown is the assumed initial neutrino spectrum (green curve); only its value at the resonance energy is important.

neutrino masses around 0.3 eV, if Z-bursts are to explain the existing UHECR AGASA spectrum. These problems are somewhat alleviated if Z-bursts are to explain the ultra-GZK events in the HiRes spectrum instead of the AGASA spectrum, as can be seen in Fig. 11.

The  $p$  and  $\gamma$  curves in Fig. 10 and Fig. 11 show the predictions of a Z-burst model computed as in Ref. [21] but with a relic neutrino mass  $m_\nu = 0.4$  eV. We assume a maximum redshift  $z_{max} = 3$  for the UHE neutrino sources (which emit only neutrinos and have not evolved), maximum intervening radio background and  $B_{EGMF} = 10^{-9}$  G. In our calculation we do not consider the effect of local inhomogeneities, such as the Virgo cluster [58]. The assumed spectrum of UHE neutrinos is shown in the figures. Only the part of this spectrum close to the resonance energy is relevant. Here we try to minimize the photon fraction predicted by Z-bursts by incorporating a low energy component of extragalactic nucleons.

In Fig. 10, a low energy component (LEC curve) parametrized as a power law (as in Eq. (1)) with index  $\alpha = 2.8$ , cutoff energy  $E_{max} = 10^{20}$  eV and a minimum

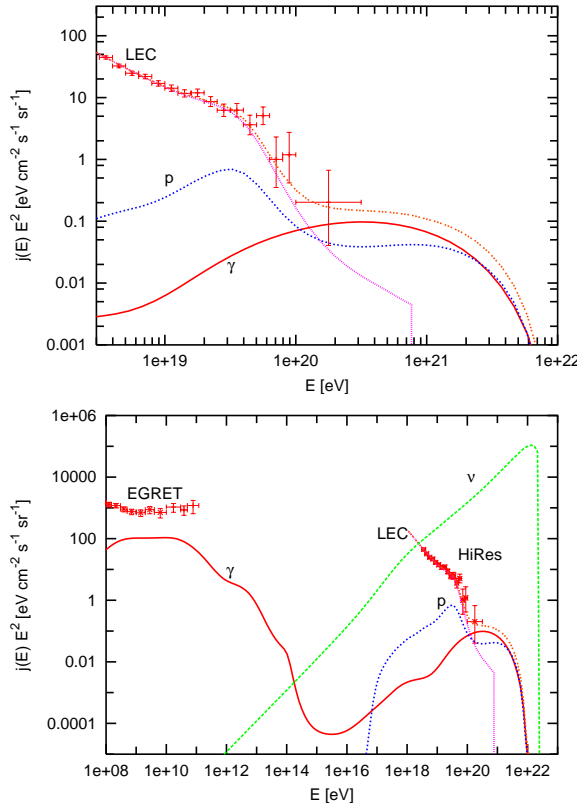


FIG. 11: As in Fig. 10 but for the HiRes data.

distance to the sources of 50 Mpc, has been added to the contribution of the Z-bursts to fit the AGASA data. The fit has minimum  $\chi^2 = 15$  for 15 bins with  $E < 10^{20}$  eV. At higher energies,  $E > 10^{20}$  eV, the fit is not good, it has a min.  $\chi^2 = 6.4$  for 3 degrees of freedom. The reason is that the predicted flux is too low at these energies. However, the fit to the spectrum above the end-point of the AGASA spectrum,  $E > 2.5 \times 10^{20}$  eV, is good: only two (mostly photon) events are predicted (where none were seen).

If we try to increase the Z-burst flux by minimizing the absorption of photons by the background, the fit is worse at high energies. If we take the lowest radio background and a small EGMF  $B = 10^{-12}$  G, the fit to the AGASA spectrum at  $E > 10^{20}$  eV is better, with min.  $\chi^2 = 4$  for 3 degrees of freedom. However, 5.8 events (mostly photons) are predicted above the AGASA end point, which we consider unacceptable.

As shown in Fig. 10b, the gamma ray flux at low energies saturates the EGRET data. Also, as shown Fig. 17a, the predicted photon fraction saturates the upper bound on the photon fraction obtained with AGASA data at  $10^{20}$  eV [51].

In Fig. 11, a low energy component (LEC curve) parametrized as a power law (see Eq. (1)) with index  $\alpha = 2.7$ , maximum energy  $E_{\max} = 10^{21}$  eV and zero minimum distance to the sources, has been added to the

contribution of the Z-bursts to fit the HiRes data. The spectrum of this model fits perfectly that of HiRes. Only 1.8 events (1 proton and 0.8 photon) are predicted above the end point of HiRes, were none were seen.

Because the super-GZK nucleon flux is here lower than with the AGASA spectrum, the predicted gamma ray flux at low energies is well under the EGRET data (see Fig. 11b). As can be seen in Fig. 17a, the predicted photon fraction is just under the upper bound obtained with AGASA data at  $10^{20}$  eV [51].

## B. Topological defects (necklaces)

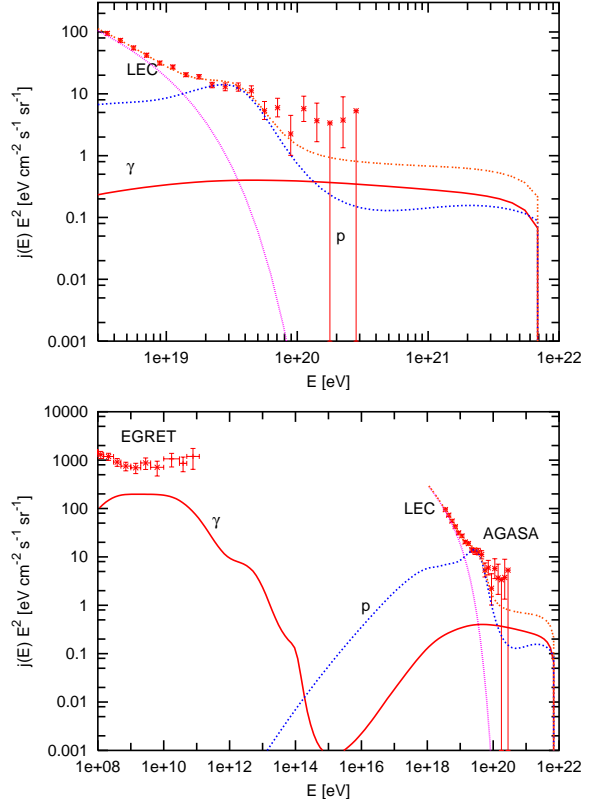


FIG. 12: Example of a fit to the AGASA spectrum with a LEC plus secondary protons and photons in a topological defect (TD) model, showing (a) the highest energies and (b) also the EGRET energy range. The LEC, as in Eq.(2), is due to nucleons from astrophysical sources. The photon over nucleon ratio in the decay products is about 3.

The curves  $p$  and  $\gamma$  in Figs. 12-13 correspond to secondary protons and photons in a particular top-down model, in which topological defects (TD), such as necklaces, produce GUT-scale mass particles, which in turn decay into quarks, leptons etc (for a review see for example Ref. [59]). The mass scale of the parent particles provides the maximum energy of the UHECR,  $E_{\max} = m_X$ , thus these scenarios avoid the difficulty in astrophysi-

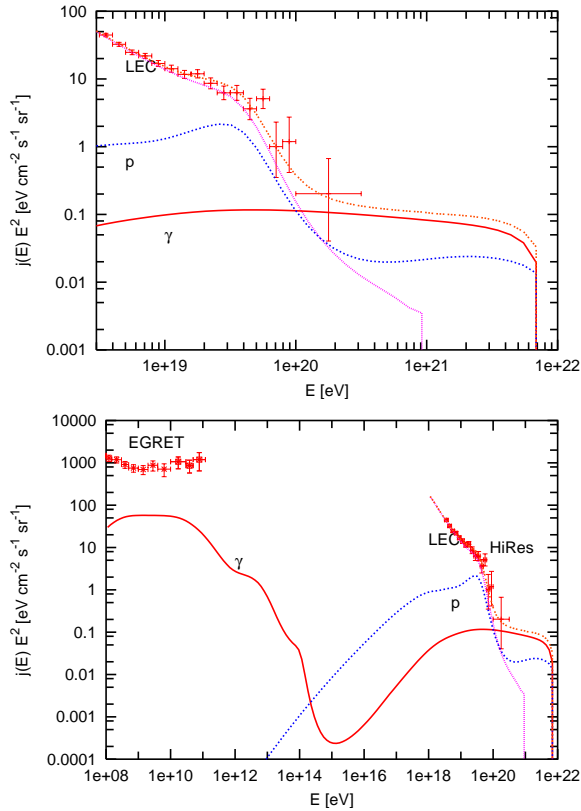


FIG. 13: As in Fig. 12 but for the HiRes spectrum.

cal objects of accelerating the UHECR to the highest energies observed. As in Z-burst models, TD scenarios predict, therefore, a new cutoff given by the parent particle mass at energies above  $10^{20}$  eV. The parent particles typically decay into leptons and quarks. The quarks hadronize, and some leptons decay resulting in a large cascade of photons, neutrinos, light leptons and a smaller amount of nucleons.

TD models may also have difficulties with the EGRET flux [45, 60] on the diffused GeV-  $\gamma$  ray background. We have taken this possible bound into account.

The TD model of Figs. 12-13 assumes a parent particle mass  $m_X = 2 \times 10^{13}$  GeV, an EGMF of  $10^{-12}$  G and the low radio background predicted by Protheroe and Biermann, which is the intermediate radio background among the three we consider in this paper. Even if we are trying to minimize the photon flux at high energies, the radio background and EGMF value are not the maximal we used in this paper. This is so because, as we show here, a smaller amount of ultra-high energy photons yields a worse fit to the AGASA data. The heavy particle injection rate is assumed to be  $\sim m_X t^{-3}$ , where  $t$  is the cosmic time.

The QCD spectrum used for Figs. 12 and 13 (shown in Fig.11 of Ref. [20]) corresponds to the decay of the heavy particles into two quarks without supersymmetry [61]. Originally, this decay model predicts a ratio of about

10 photons per nucleon in the decay products (as does Ref. [62]), while in more recent models [63, 64, 65] this ratio is only 2 - 3. So, for Fig. 12 and Fig. 13 the ratio was brought to be equal to 3. Here we fit the LEC with the function in Eq. (2) with  $\beta = 2.7$  and an exponential energy cut with  $E_{\text{cut}} = 8 \times 10^{19}$  eV, in order to increase the contribution of the TD model to the AGASA flux, which is still too low at high energies. Again, at energies  $E < 10^{20}$  eV the fit is good, with minimum  $\chi^2 = 14$  for 15 degrees of freedom. However, the fit of the AGASA spectrum above the GZK energy is bad, with minimum  $\chi^2 = 7.4$  per 3 degrees of freedom. This is due to the strong reduction of the TD flux above the GZK energy (due to the GZK effect, because there are more protons than in Fig. ??), which means that in order to have a good fit at energies below the GZK energy, the flux is too small at higher energies. Now, there are only 3.7 events at  $E > 10^{20}$  eV (of which 2.7 are photons), while AGASA observed 11 events. But, if we take the minimum radio background (not shown in figures) instead of the intermediate one we use for the figures, the fit to the AGASA occupied bins above the GZK energy is good (with minimum  $\chi^2 = 2.2$  per 3 degrees of freedom), but the number of events predicted above the end-point of the AGASA spectrum (where no events were observed) becomes 10, which is again unacceptable.

From Fig. 12 we conclude that the representative TD models we study are barely consistent with the AGASA data. They either predict a flux too low at super-GZK energies or too many events above the highest energy events observed by AGASA. For the TD curve in Fig. 17a the model of Fig. 12 was used. We see in Fig. 17a that the predicted photon ratio is somewhat above the upper bound on the photon fraction obtained with AGASA data at  $10^{20}$  eV [51].

In Fig. 13, a low energy component (LEC curve), parametrized as a power law (see Eq. (1)) with index  $\alpha = 2.7$  and cutoff energy  $E_{\text{max}} = 10^{21}$  eV and zero minimum distance to the sources, has been added to the contribution of the TD model to fit the HiRes data. The spectrum of this model (with a  $\gamma/p$  ratio of 3) fits well the HiRes data. This model predicts 0.4 events above the end point of the HiRes spectrum. It is clear that the fit would be good too with a larger  $\gamma/p$  ratio in the TD decay products, since one can redistribute the protons between the LEC and the TD contribution without a significant change in the fit (but the photon fraction at the highest energies would be somewhat larger).

As mentioned above the QCD model used so far in this subsection predicts a ratio of about 10 photons per nucleon in the decay products [61] (although we brought it artificially to 3) while in more recent models [63, 64, 65] this ratio is considerably smaller. We include here also the results obtained with one of these more recent models. The heavy particle decay spectrum used in Fig. 14 corresponds to the decay of the heavy particles into quark

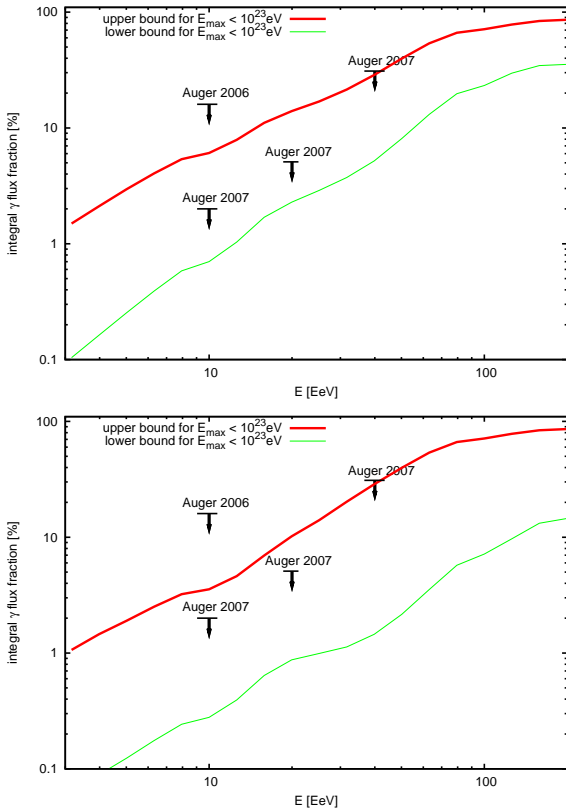


FIG. 14: Maximum and minimum GZK photon fractions in the integral flux above the energy  $E$  for the topological defect (TD) model described in the text and with (a) the AGASA spectrum (upper panel) and (b) the HiRes spectrum (lower panel). The 2006 [71] and 2007 [72] Auger upper bounds on the photon fraction are also shown.

and antiquark pairs with the ‘‘gaugino set of supersymmetric parameters’’ taken from Ref. [64]. We choose this particular decay mode because it is one in which the initial number of photons per nucleon produced is one of the lowest (since we want to estimate the minimum GZK photon flux produced). This decay model predicts a ratio of about 2 or less photons per nucleon in the decay products. At low energies the fragmentation functions were suppressed following Fig. 2.11 of Ref. [66]. For  $(E/E_{\max}) < R_o$  the suppression factor used is  $R^{-\log_{10}(R/W^2)}$ , where  $R = R_o/(E/E_{\max})$  and  $W$  is the width in decades at which the spectrum is suppressed by a factor 0.1 (for  $(E/E_{\max}) > R_o$  there is no suppression). From the figure just mentioned, one can find the values of the parameters  $R_o$  and  $W$ . We used  $R_o = 10^{-6}$  and  $W = 3.5$ .

Fig. 14 shows the maximum and minimum photon fractions found using the method of Ref. [67] for  $E_{\max} < 10^{23}$  eV. In Ref. [67] the maximum and minimum GZK photon fractions were found assuming a power law spectrum of protons is injected by astrophysical sources and fitting the AGASA and HiRes UHECR spectra for ener-

gies  $E > 4 \times 10^{19}$  eV. It was also assumed that any possible low energy component is irrelevant at this energies. Notice that the LEC in Fig. 12 fulfills this latter condition but that in Fig. 13 does not. To produce Fig. 14 we use the same procedure but replace the injected spectrum by that produced in the heavy particle decay. We choose the value of the amplitude of the injected spectrum by maximizing the Poisson likelihood function using the UHECR data from  $4 \times 10^{19}$  eV up to the last published bin of each spectrum plus one extra bin with zero observed events at higher energies. This extra bin and the highest energy empty published bins, take into account the non-observation of events above the highest occupied energy bin in the data of each collaboration, the end-point energy of each spectrum (i.e. at  $E > 2.3 \times 10^{20}$  eV for AGASA [68] and  $E > 1.6 \times 10^{20}$  eV for HiRes [69]), although their aperture remains constant with increasing energy. We then compute using a Monte Carlo technique the goodness of the fit, or  $p$ -value, of the distribution. Only the models with goodness of fit  $p$ -value larger than 0.05 are considered, as in Ref. [67]. The maximum and minimum GZK photon fluxes depend on the intervening radio background and EGMF  $B$  and on the value of  $E_{\max} = m_X/2$ . The 2006 [71] and 2007 [72] Auger upper bounds on the photon fraction are also shown in Fig. 14. The models with the minimal photon fraction for the AGASA spectrum change with energy. For  $E < 1.3 \times 10^{20}$  eV the minimum photon fraction results from choosing  $E_{\max} = 8 \times 10^{22}$ , intermediate radio background and  $B = 10^{-9}$  G, while for  $E > 1.3 \times 10^{20}$  eV the model with minimum photon fraction has the same  $E_{\max}$  but maximal radio background, and  $B = 10^{-11}$  G. The model with the minimal photon fraction for the HiRes spectrum has also  $E_{\max} = 8 \times 10^{22}$  and maximal radio background but  $B = 10^{-9}$  G.

### C. Super Heavy Dark Matter (SHDM)

In this scenario super heavy metastable particles are produced in early Universe, and they remain at present. They form part of the dark matter of the Universe and, in particular of the dark halo of our galaxy. These particles (with colorful names such as ‘cryptons’ or ‘wimpzillas’) may decay [73, 74, 75] or annihilate [76] into the observed UHECR. The spectra of the decay or annihilation products are essentially determined by the physics of QCD fragmentation and this implies photon domination of the flux at the highest energies.

The UHECR in these models are produced predominantly within the dark halo of our own galaxy. Thus these models predict an excess of UHECR events from the galactic center [77]. This anisotropy is in conflict with the data on arrival directions of the SUGAR experiment [78], unless SHDM are responsible for the majority of UHECR events only at energies above  $6 \times 10^{19}$  eV [79].

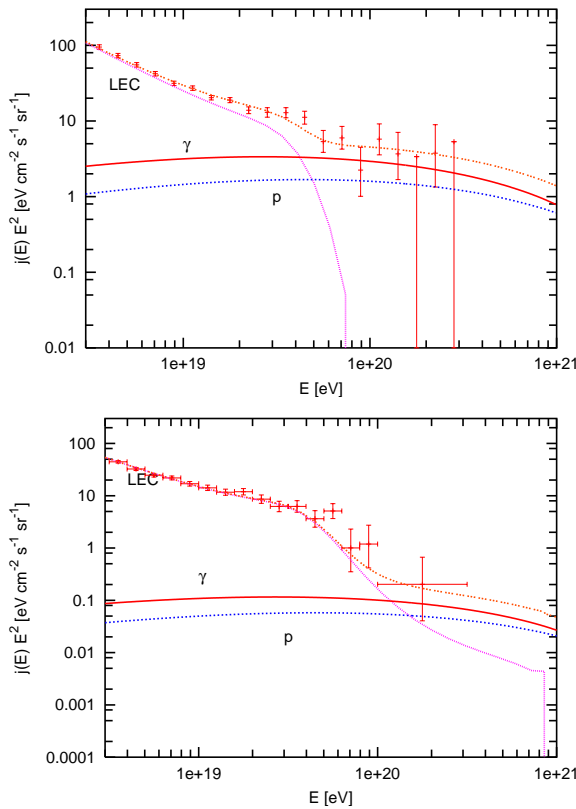


FIG. 15: Example of a fit (a) to AGASA (upper panel) and (b) HiRes (lower panel) data at high energies with a LEC plus protons and photons decay products in a super heavy dark matter model. The parent particle mass is  $2 \times 10^{12}$  GeV. The low energy component (LEC) is due to nucleons from astrophysical sources.

Even in this case, annihilating SHDM models are disfavored at least at the 99% C.L. by the SUGAR data, while decaying SHDM models have a probability of  $\sim 10\%$  to be consistent with the SUGAR data [79].

As seen in Fig. 17a the model we present is barely consistent with the upper bound on the photon fraction obtained with AGASA data at  $10^{20}$  eV [51].

The  $p$  and  $\gamma$  curves in Fig. 15 are the predictions of a supersymmetric SHDM model taken from a recent calculation in Ref. [65], obtained by averaging over all possible decay channels, including decays into quarks, squarks, gluons and gluinos. These predictions we use here as an example, are similar to those of previous calculations [63] (see Fig. 17 of Ref. [65]). In particular, the ratio of SHDM produced photons over nucleons is about 2.

Here we reduced the mass of the parent particle to  $m_X = 2 \times 10^{12}$  GeV because, with the  $10^{14}$  GeV mass used in Ref. [65] to fit the AGASA data, we find that too many events are predicted above the end point of the AGASA spectrum. To be more precise, the model of Fig. 15, with  $m_X = 2 \times 10^{12}$  GeV, predicts 3.0 events above the end-point of the AGASA spectrum, i.e. at

$E > 2.5 \times 10^{20}$  eV. The fit has a min.  $\chi^2 = 2$  for the 3 occupied bins at energies  $E > 10^{20}$  eV.

For  $m_X = 10^{14}$  GeV, as used in Ref. [65], the SHDM model predicts instead 8.5 events above the AGASA end-point. With the HiRes spectrum, there would not be any problem in using the higher  $m_X$ , since only 0.16 events are predicted with  $m_X = 2 \times 10^{12}$  GeV and 0.8 events are predicted with  $m_X = 10^{14}$  GeV above the HiRes end-point (i.e. at  $E > 3.2 \times 10^{20}$  eV).

We can turn this argument around and set a bound on the SHDM mass by requiring that no more than, say, 3 events are predicted above the end-point of the AGASA spectrum. At the 95% C.L. this limit is  $m_X < 2 \times 10^{21}$  eV. This should be taken as an order of magnitude limit, because AGASA assigned an energy to the events assuming proton primaries and for photon primaries the energy of some of the highest energy events can be higher [80]. A way to alleviate this bound, at the expense of reducing the goodness of the fit, is to reduce the contribution of the SHDM model to the total UHECR spectrum. For example, one could allow for  $m_X = 10^{14}$  GeV by reducing by force the SHDM contribution above the AGASA end-point to 3 events. In this case only 7 events would be predicted at  $E > 10^{20}$  eV, where AGASA observed 11. The fit has a min.  $\chi^2 = 6.7$  for the 3 occupied bins at energies  $E > 10^{20}$  eV. Thus, reducing the contribution of the SHDM flux to the AGASA flux to allow for larger  $m_X$  values brings SHDM models close to just extragalactic protons with a hard spectrum  $\sim 1/E$ , (with min.  $\chi^2 = 7.8$ , see subsection III.A) in terms of goodness of fit.

The nucleon and photon spectra produced by the SHDM model we use is too hard, thus an additional low energy component (LEC), which we assume consists of extragalactic nucleons, is needed to fit the data. In Fig. 15a, a LEC, parametrized as a power law (see Eq. (1)) with index  $\alpha = 2.8$ , maximum energy  $E_{\max} = 10^{20}$  eV, and with a zero minimum distance to the sources, has been added to the contribution of the SHDM model to fit the AGASA data. In Fig. 15b, the LEC shown, added to fit the HiRes spectrum, has  $\alpha = 2.7$ ,  $E_{\max} = 10^{21}$  eV and an assumed zero minimum distance to the sources.

Note that the SHDM model studied so far, with the AGASA spectrum predicts a significant photon fraction, about 10-20 %, at energies  $E > 10^{19}$  eV (see Fig. 17a) which are too high for the recent Auger limits on the the photon component of the UHECR. We discuss this issue in the following section.

Using the statistical method of Ref. [67] and the heavy particle decay spectrum used in Fig. 14 (taken from Refs. [64, 66]- see the explanations in the last paragraph of the previous subsection) we fitted the UHECR spectrum above  $4 \times 10^{19}$  eV just with the spectrum resulting from the superheavy particle decay, with no absorption or redshift, and obtained the maximum and minimum pho-

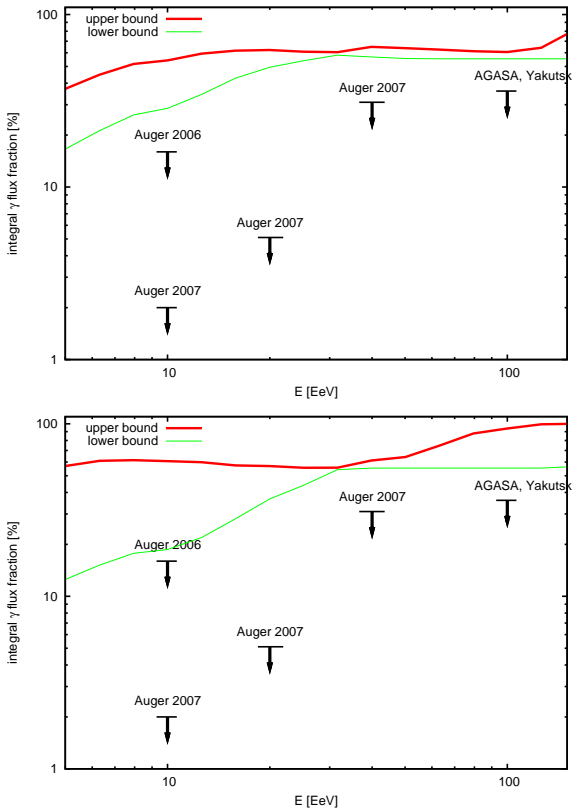


FIG. 16: Maximum and minimum GZK photon fractions in the integral flux above the energy  $E$  for the SHDM model with the fragmentation function of Ref. [64] mentioned in Sect. IV B using the statistical method of Ref. [67] and with (a) the AGASA spectrum (upper panel) and (b) the HiRes spectrum (lower panel). The 2006 [71] and 2007 [72] Auger upper bounds on the photon fraction are also shown.

ton fractions of the integrated flux shown in Fig. 16. We assumed that the LEC is negligible at energies  $4 \times 10^{19}$  eV and above. Notice that the LEC in Fig. 15b, chosen above to fit the HiRes spectrum, violates this assumption (what leads to lower predicted photon levels, since the SHDM model dominates only at higher energies). In SHDM models the maximum and minimum photon fractions depend only on the value of  $E_{\max} = m_X/2$  and for each energy  $E$  the values of  $E_{\max}$  giving the maximum of the minimum photon ratio are different. We considered the range  $1 \times 10^{20}$  eV  $< E_{\max} < 1 \times 10^{23}$  eV. However the fitting procedure shows that only the ranges  $3.5 \times 10^{20}$  eV  $< E_{\max} < 1.4 \times 10^{21}$  eV and  $1.2 \times 10^{20}$  eV  $< E_{\max} < 7.1 \times 10^{20}$  eV provide acceptable models.

Notice that when the spectrum of SHDM is assumed to dominate the UHECR spectrum only at the highest energies, i.e. close the  $10^{20}$  eV as is the case of the model in Fig. 15b, the resulting minimum photon fractions are smaller (about 1% at  $1 \times 10^{19}$  eV - see Fig. 17b) while if SHDM are assumed to reproduce the UHECR spectrum already at  $4 \times 10^{19}$  eV and above, the minimum expected

photon fractions are larger (above 10% at  $1 \times 10^{19}$  eV - see Fig. 17b).

#### D. Photon fractions

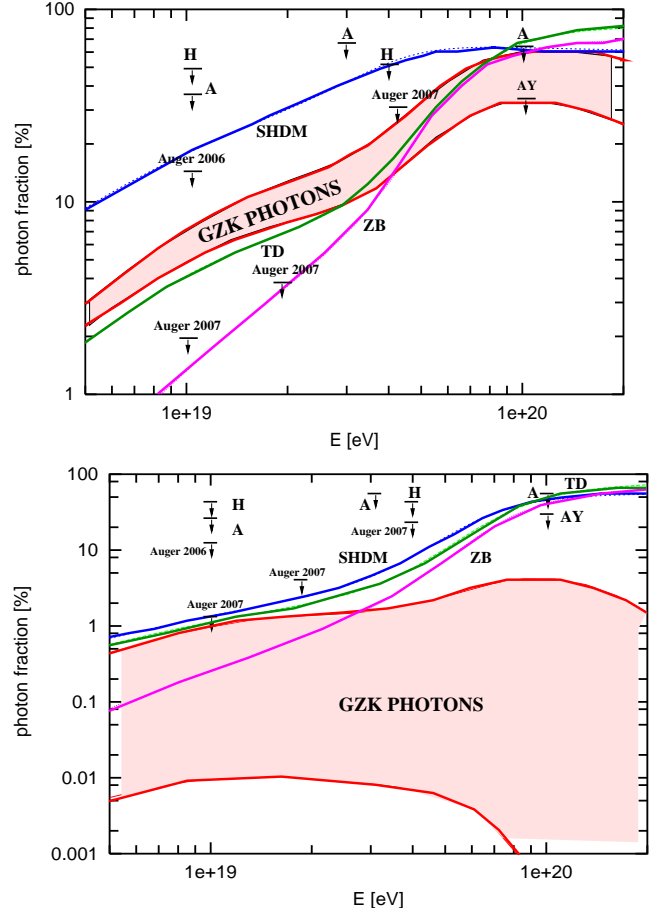


FIG. 17: Photon fraction in percentage of the total predicted integrated UHECR spectrum above the energy  $E$  for (a) the AGASA spectrum (upper panel) and (b) the HiRes spectrum (lower panel). The pink regions show the range of GZK photon fractions expected if only nucleons are produced at the sources (see Sect. III). The curves labeled ZB (Z-bursts), TD (topological defects) and SHDM (Super Heavy Dark Matter model) show examples of minimum photon fractions predicted by these models (see Sect. IV). Upper limits: **A** from AGASA, Ref. [10] at  $1-3 \times 10^{19}$  eV, Ref [51] and obtained with AGASA data at  $10^{20}$  eV; **AY** from the Yakutsk collaboration combining data from Yakutsk and AGASA, above  $1 \times 10^{20}$  eV [70]; **H** from Haverah Park [18]. The 2006 [71] and 2007 [72] Auger upper bounds on the photon fraction are also shown.

In Fig. 17 we compare the range of GZK photon fractions we obtained in section III with the minimal photon fractions predicted by the Top-Down models shown in Figs. 10 to 13 and 15 and existing experimental upper bounds. Fig. 17 shows the fraction of photons as percentage of the total predicted integrated UHECR flux

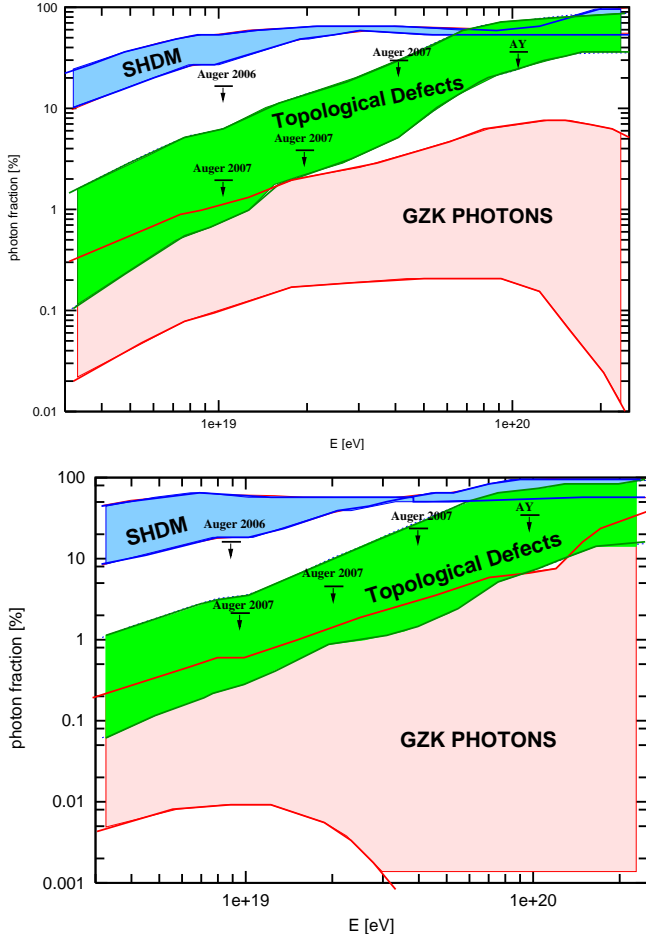


FIG. 18: Photon fraction in percentage of the total predicted integrated UHECR spectrum above the energy  $E$  for (a) the AGASA spectrum (upper panel) and (b) the HiRes spectrum (lower panel). Shown in pink is the wider range of GZK photon fractions expected if only nucleons are produced at the sources derived in Ref. [67] (see Fig. 7 therein). Shown in green and blue are respectively the ranges of photon fractions in Fig. 14 (for TD models) and in Fig. 16 (for SHDM models) also obtained with the method of Ref. [67] (see the last paragraphs of IV.B and IV.C). The 2006 [71] and 2007 [72] Auger upper bounds on the photon fractions as well as the upper bound by the Yakutsk collaboration combining data from Yakutsk and AGASA, above  $1 \times 10^{20}$  eV [70] (**AY**) are also shown.

above the energy  $E$  in every model.

In Fig. 17a and b the AGASA spectrum and the HiRes spectrum are assumed, respectively. The ZB, TD and SHDM curves in Fig. 17 correspond to the Z-burst, topological defects and super heavy dark matter models in Figs. 10 to 13 and 15. The pink bands show the range of GZK photons between the maximum and minimum fluxes obtained in Sect. III. The upper and lower boundaries of the pink band in Fig. 17a are the photon curve in Fig. 6b and photon curve in Fig. 7b, respectively. The upper and lower boundaries of the pink band in Fig. 17b

are the highest photon curve in Fig. 8b and the lowest photon curve of Fig. 9b, respectively. Notice how the GZK photon band depends on the assumed spectrum: the band for AGASA is above the band for HiRes, entirely separated from it.

In Fig. 18 we compare the range of GZK photon fractions derived in Ref. [67] with nucleons injected by the sources, with the maximum and minimum photon fractions in topological defects (necklaces) and superheavy dark matter models shown in Figs. 14 and 16. These were obtained with the same method of Ref. [67] and the heavy particle decay model described in the last paragraphs of the subsections IV.B and IV.C.

From Fig. 17 and Fig. 18 we conclude that at energies above  $3 \times 10^{19}$  eV the minimum photon fraction predicted by Top-Down models is either larger or at most comparable to the maximum expected GZK photon ratio and the 2007 Auger [72] and the Agasa-Yakutsk [70] upper bounds on the photon fraction strongly constrain Top-Down models, in particular SHDM models.

The differences between Figs. 17 and 18 are due to the different methods and models with which the photons fractions were derived. The GZK photon fractions for the AGASA spectrum are lower in Fig. 18 than in Fig. 17 because of the different fitting procedure and the different choice of  $E_{\max}$  which can be only as high as  $10^{21}$  eV in Ref. [67], a more conservative value, instead of  $10^{22}$  eV, the preferred value for the AGASA spectrum in Section III.

The SHDM photon fractions are much higher in Fig. 18 than in Fig. 17. The superheavy particle fragmentation functions used to produce both figures are similar and the differences in the minimum photon fraction expected are due to the range of energies at which the SHDM is assumed to provide the bulk of UHECR: in Fig. 18 it is above  $4 \times 10^{19}$  eV and in Fig. 17 it is instead starting at energies closer to  $10^{20}$  eV. However, in both cases the SHDM models studied either saturate or exceed the 2007 Auger bounds, in particular that at  $1 \times 10^{19}$  eV, and the Agasa-Yakutsk bound at  $1 \times 10^{20}$  eV. Thus, the Auger bounds by themselves already exclude as the dominant mechanism to produce UHECR the SHDM models considered here except at energies very close to  $10^{20}$  eV [81]. Also the photon fractions given in Fig. 2 of Ref. [82] are rejected by the 2007 Auger bound at  $1 \times 10^{19}$  eV. There is another type of SHDM models [83] in which the photon fraction can be smaller. Those with the smallest photon fractions among tend to correspond to superheavy particles with larger mass and the constraint on the events predicted above experimental end point is important. Some of these models are still allowed but very close to the existing photon limits, within a factor of two or so [84].

The topological defects models used in Figs. 17 and 18 are different, that of Fig. 18 being in line with the more recent estimates of fragmentation functions in which the photon fraction is smaller than in older models. This is

the main reason for the minimal photon ratios expected in these models to be smaller in Fig 18 than in Fig 17. These models are not ruled out by present photon fraction bounds however the photon fractions they predict are above 10% at  $1 \times 10^{20}$  eV. The present Agasa-Yakutsk limit upper limit of  $N_\gamma/N_{\text{tot}} < 36\%$  strongly limits these models. So, either UHECR photons at energies close to  $10^{20}$  eV will be detected, or better experimental limits will be obtained in the future by Auger. An upper limit close to 10% at those energies, would reject all Top-Down models as the origin of UHECR.

Thus, the photon fraction at energies above  $10^{19}$  eV, is a crucial test for Top-Down models. The only caveat to this conclusion resides in considering that the evaluation [35] of the extragalactic radio background could be wrong by several orders of magnitude, so that this background could be larger than those of Ref. [35] by a large factor of 30 to 100 as suggested in Ref. [85], although there are no specific arguments at present to justify these large factors.

We have shown in this paper that either the detection of UHECR photons or an improvement of the existing upper limits on the photon flux, is very important, both for Top-Down as well as for Bottom-Up mechanisms to explain the UHECR. SHDM and Z-burst models seem to be strongly disfavored by the present experimental upper bounds on photon fraction. With astrophysical sources, the GZK photon flux is important to understand the initial proton or neutron spectrum emitted at the UHECR sources and the distribution of sources. UHECR photons may help us to understand the intervening extragalactic magnetic fields and radio background. We have presented fits to both the AGASA and the HiRes UHECR spectra with extragalactic nucleons, the GZK photons they produce and, when needed, an additional low energy component at energies below  $10^{19}$  eV (see section III). The band of expected GZK photon flux depends clearly on the UHECR spectrum and also on the assumptions and procedure used (see Figs. 17 and 18). Once the particular UHECR spectrum is fixed, the uncertainties in this flux due to the extragalactic nucleon model and due to our ignorance of the intervening background are comparable (see subsection II.E). Thus, extracting information on the extragalactic nucleon flux from the GZK photons would require to have independent information on the extragalactic magnetic fields and radio background, and vice versa.

The detection of UHECR photons would open a new window for ultra-high energy astronomy and help establish the UHECR sources.

### Acknowledgments

We thank I. Tkachev for fruitful discussions and suggestions at early stages of this work. We also thank S. Troitsky for careful reading of the manuscript and for several important suggestions and corrections. This work

was supported in part by NASA grants NAG5-13399 and ATP03-0000-0057. G.G was supported in part by the US DOE grant DE-FG03-91ER40662 Task C.

---

- [1] K. Greisen, Phys. Rev. Lett. **16**, 748 (1966). G. T. Zatsepin and V. A. Kuzmin, JETP Lett. **4**, 78 (1966) [Pisma Zh. Eksp. Teor. Fiz. **4**, 114 (1966)].
- [2] M. Takeda *et al.*, Phys. Rev. Lett. **81**, 1163 (1998), [astro-ph/9807193]; see N. Hayashida *et al.*, astro-ph/0008102, for an update; see also <http://www-akeno.icrr.u-tokyo.ac.jp/AGASA/>.
- [3] R. U. Abbasi *et al.* [High Resolution Fly's Eye Collaboration], Phys. Rev. Lett. **92**, 151101 (2004) [arXiv:astro-ph/0208243]. see also <http://hires.physics.utah.edu/>.
- [4] F.W. Stecker, Phys. Lett. **21**, 1016 (1968); S. Yoshida and M. Teshima, Prog. Theor. Phys. **89**, 833 (1993); F. A. Aharonian and J. W. Cronin, Phys. Rev. **D50**, 1892 (1994); J. W. Elbert and P. Sommers, Astrophys. J. **441**, 151 (1995);
- [5] F. Halzen, R. A. Vazquez, T. Stanev, and V. P. Vankov, Astropart. Phys., **3**, 151 (1995).
- [6] K. Dolag, D. Grasso, V. Springel and I. Tkachev, JETP Lett. **79**, 583 (2004) [Pisma Zh. Eksp. Teor. Fiz. **79**, 719 (2004)] [arXiv:astro-ph/0310902]; and JCAP **0501**, 009 (2005) [arXiv:astro-ph/0410419].
- [7] G. Sigl, F. Miniati and T. A. Ensslin, Phys. Rev. D **68**, 043002 (2003) [arXiv:astro-ph/0302388]; arXiv:astro-ph/0309695; Phys. Rev. D **70**, 043007 (2004) [arXiv:astro-ph/0401084]. arXiv:astro-ph/0409098.
- [8] G. Archibald and P. V. Sokolsky [HiRes Collaboration], *Prepared for 28th International Cosmic Ray Conferences (ICRC 2003), Tsukuba, Japan, 31 Jul - 7 Aug 2003*
- [9] D. R. Bergman [The HiRes Collaboration], Nucl. Phys. Proc. Suppl. **136**, 40 (2004) [arXiv:astro-ph/0407244].
- [10] K. Shinozaki *et al.*, *Prepared for 28th International Cosmic Ray Conferences (ICRC 2003), Tsukuba, Japan, 31 Jul - 7 Aug 2003*
- [11] T. T. Stanev, Astrophys. J. **479**, 290 (1997) [arXiv:astro-ph/9607086]; G. A. Medina-Tanco, E. M. de Gouveia Dal Pino and J. E. Horvath, arXiv:astro-ph/9707041; M. Prouza and R. Smida, arXiv:astro-ph/0307165.
- [12] J.L. Puget, F. W. Stecker and J. Bredekamp Astrophys. J. **205**, 638 (1976)
- [13] L. N. Epele and E. Roulet, Phys. Rev. Lett. **81**, 3295 (1998); and JHEP **9810**, 009 (1998); see also F. Stecker, Phys. Rev. **180**, 1264 (1969); F. W. Stecker and M. H. Salamon, Astrophys. J. **512**, 521 (1999)
- [14] G. Bertone, C. Isola, M. Lemoine and G. Sigl, Phys. Rev. D **66**, 103003 (2002) [arXiv:astro-ph/0209192].
- [15] V. Berezinsky, A. Z. Gazizov and S. I. Grigorieva, arXiv:hep-ph/0204357.
- [16] Pierre Auger Observatory, <http://www.auger.org>.
- [17] K. Shinozaki *et al.*, Astrophys. J. **571** (2002) L117.
- [18] M. Ave, J. A. Hinton, R. A. Vazquez, A. A. Watson and E. Zas, Phys. Rev. Lett. **85**, 2244 (2000) [arXiv:astro-ph/0007386]; Phys. Rev. D **65**, 063007 (2002) [arXiv:astro-ph/0110613].
- [19] V. S. Berezinsky and G. T. Zatsepin, Phys. Lett **28B**,

423 (1969).

[20] O. E. Kalashev, V. A. Kuzmin, D. V. Semikoz and G. Sigl, Phys. Rev. D **66**, 063004 (2002);

[21] D. V. Semikoz and G. Sigl, JCAP **0404**, 003 (2004).

[22] <http://icecube.wis.edu/>.

[23] ANtarctic Impulse Transient Array (ANITA), <http://www.ps.uci.edu/~anita/>.

[24] Saltdome Shower Array, P. Gorham *et al.*, Nucl. Instrum. Meth. A **490**, 476 (2002).

[25] Extreme Universe Space Observatory, <http://www.euso-mission.org/>.

[26] Orbiting Wide-angle Light-collectors, <http://owl.gsfc.nasa.gov/>.

[27] J. Wdowczyk , W. Tkaczyk, C. Adcock and A. W. Wolfendale, J. Phys. A: Gen. Phys **4** L37-9 (1971); J. Wdowczyk , W. Tkaczyk and A. W. Wolfendale, J. Phys. A: Gen. Phys **5** 1419 (1972); J. Wdowczyk and A. W. Wolfendale, Astrophys. Jour. **349**, 35 (1990)

[28] F.A. Aharonian, V.V. Vardanian and B.L. Kanevsky, Astrophysics and Space Science **167**, 111 (1990); Corresponding proton GZK cutoff calculation was done in *ibid* **93**, 111 (1990).

[29] S. j. Lee, A. Olinto and G. Sigl, Astrophys. J. **455**, L21 (1995) [arXiv:astro-ph/9508088].

[30] O. E. Kalashev, V. A. Kuzmin, D. V. Semikoz and I. I. Tkachev, arXiv:astro-ph/0107130.

[31] P. G. Tinyakov and I. I. Tkachev, JETP Lett. **74**, 445 (2001) [Pisma Zh. Eksp. Teor. Fiz. **74**, 499 (2001)] [arXiv:astro-ph/0102476].

[32] O.E. Kalashev, V.A. Kuzmin and D.V. Semikoz, astro-ph/9911035. O.E. Kalashev, V.A. Kuzmin and D.V. Semikoz, astro-ph/0006349.

[33] P. Bhattacharjee, G. Sigl, Phys. Rept. **327**, 109 (2000);

[34] T. A. Clark, L. W. Brown, and J. K. Alexander, Nature **228**, 847 (1970).

[35] R. J. Protheroe and P. L. Biermann, Astropart. Phys. **6**, 45 (1996) [Erratum-*ibid.* **7**, 181 (1997)]

[36] J. R. Primack, R. S. Somerville, J. S. Bullock and J. E. G. Devriendt, AIP Conf. Proc. **558**, 463 (2001) [arXiv:astro-ph/0011475].

[37] P. P. Kronberg, Rept. Prog. Phys. **57**, 325 (1994); D. Ryu, H. Kang and P. L. Biermann, Astron. Astrophys. **335**, 19 (1998) [arXiv:astro-ph/9803275]; P. Blasi, S. Burles and A. V. Olinto, Astrophys. J. **514**, L79 (1999) [arXiv:astro-ph/9812487].

[38] K. Dolag, M. Bartelmann and H. Lesch, Astron. & Astrophys. **387**, 383 (2002) [arXiv:astro-ph/0202272].

[39] A. M. Hillas, Ann. Rev. Astron. Astrophys. **22**, 425 (1984).

[40] V. S. Berezinsky, et al, “*Astrophysics of Cosmic Rays.*” (North-Holland, Amsterdam, 1990); T.K. Gaisser, “*Cosmic Rays and Particle Physics.*” (Cambridge University Press, Cambridge, England, 1990).

[41] R.J. Protheroe, In “*Topics in cosmic-ray astrophysics*”, ed. M. A. DuVernois, Nova Science Publishing: New York, 1999, (astro-ph/9812055); M.A. Malkov, Ap.J. **511**, L53 (1999); K. Mannheim, R.J. Protheroe, J. P. Rachen, Phys. Rev. **D63**, 023003 (2001).

[42] E. V. Derishev, F. A. Aharonian, V. V. Kocharovskiy and V. V. Kocharovskiy, Phys. Rev. D **68**, 043003 (2003) [arXiv:astro-ph/0301263].

[43] A. Neronov and D. Semikoz, New Astronomy Reviews **47**, 693 (2003); A. Neronov, P. Tinyakov and I. Tkachev, arXiv:astro-ph/0402132.

[44] V. Berezinsky, A. Z. Gazizov and S. I. Grigorieva, arXiv:astro-ph/0210095.

[45] P. Sreekumar *et al.* [EGRET Collaboration], Astrophys. J. **494**, 523 (1998) [arXiv:astro-ph/9709257].

[46] M. Takeda *et al.*, Astrophys. J. **522**, 225 (1999) [arXiv:astro-ph/9902239].

[47] R. U. Abbasi *et al.* [The High Resolution Fly’s Eye Collaboration (HIRES)], Astrophys. J. **610**, L73 (2004) [arXiv:astro-ph/0404137].

[48] R. U. Abbasi *et al.* [The High Resolution Fly’s Eye Collaboration], arXiv:astro-ph/0412617.

[49] H. Yoshiguchi, S. Nagataki and K. Sato, “Statistical significance of small scale anisotropy in arrival directions of ultra-high energy cosmic rays,” astro-ph/0404411; M. Kachelriess and D. Semikoz, arXiv:astro-ph/0405258.

[50] E. Waxman, K. B. Fisher and T. Piran, Astrophys. J. **483**, 1 (1997) [astro-ph/9604005]. S. L. Dubovsky, P. G. Tinyakov and I. I. Tkachev, Phys. Rev. Lett. **85**, 1154 (2000) [astro-ph/0001317]. Z. Fodor and S. D. Katz, [hep-ph/0007158]. H. Yoshiguchi, S. Nagataki, S. Tsubaki and K. Sato, Astrophys. J. **586**, 1211 (2003) [Erratum-*ibid.* **601**, 592 (2004)] [astro-ph/0210132]. H. Yoshiguchi, S. Nagataki and K. Sato, Astrophys. J. **592**, 311 (2003) [astro-ph/0302508]. P. Blasi and D. De Marco, Astropart. Phys. **20**, 559 (2004) [arXiv:astro-ph/0307067].

[51] P. Homola *et al.*, arXiv:astro-ph/0411060; M. Risse *et al.*, arXiv:astro-ph/0502418.

[52] T. J. Weiler, Phys. Rev. Lett. 49 (1982) 234 . Astrophys. J. 285 (1984) 495; D. Fargion, B. Mele and A. Salis, Astrophys. J. 517 (1999) 725 [astro-ph/9710029]. T. J. Weiler, Astropart. Phys. 11 (1999) 303 [hep-ph/9710431].

[53] Z. Fodor, S. D. Katz and A. Ringwald, Phys. Rev. Lett. **88**, 171101 (2002) [hep-ph/0105064] and JHEP **0206**, 046 (2002) [hep-ph/0203198].

[54] O. E. Kalashev, V. A. Kuzmin, D. V. Semikoz and G. Sigl, Phys. Rev. D 65 (2002) 103003 [arXiv:hep-ph/0112351].

[55] P. W. Gorham, K. M. Liewer, C. J. Naudet, D. P. Saltzberg and D. R. Williams, astro-ph/0102435; P. Gorham, C. Hebert, K. Liewer, C. Naudet, D. Saltzberg, D. Williams, astro-ph/0310232.

[56] N. Lehtinen, P. Gorham, A. Jacobson, R. Roussel-Dupre, Phys. Rev. D **69** (2004) 013008.

[57] G. Gelmini, G. Varieschi and T. J. Weiler, Phys. Rev. D **70**, 113005 (2004) [arXiv:hep-ph/0404272].

[58] A. Ringwald, T. J. Weiler and Y. Y. Wong, arXiv:astro-ph/0505563.

[59] P. Bhattacharjee and G. Sigl, Phys. Rept. **327**, 109 (2000) [arXiv:astro-ph/9811011].

[60] A. W. Strong, I. V. Moskalenko and O. Reimer, Astrophys. J. **613**, 956 (2004) [arXiv:astro-ph/0405441].

[61] V.A. Khoze and W. Ochs, Int. J. Mod. Phys. A **12** 2949 (1997).

[62] V. Berezinsky and M. Kachelriess, Phys. Rev. D **63**, 034007 (2001) [arXiv:hep-ph/0009053].

[63] S. Sarkar and R. Toldra, Nucl. Phys. **B621**, 495 (2002); C. Barbot and M. Drees, Phys. Lett. B **533**, 107 (2002) and Astropart. Phys. **20** 5 (2003).

[64] C. Barbot and M. Drees, Phys. Lett. B **533**, 107 (2002) and Astropart. Phys. **20** 5 (2003).

[65] R. Aloisio, V. Berezinsky and M. Kachelriess, Phys. Rev. D **69**, 094023 (2004) [arXiv:hep-ph/0307279].

- [66] C. Barbot, hep-ph/0308028.
- [67] G. B. Gelmini, O. Kalashev and D. V. Semikoz, arXiv:0706.2181 [astro-ph].
- [68] M. Takeda *et al.*, Astropart. Phys. **19**, 447 (2003) [astro-ph/0209422].
- [69] R. Abbasi *et al.* [HiRes Collaboration], astro-ph/0703099.
- [70] G. I. Rubtsov *et al.*, Phys. Rev. D **73**, 063009 (2006).
- [71] J. Abraham *et al.* [Pierre Auger Collaboration], Astropart. Phys. **27**, 155 (2007) [arXiv:astro-ph/0606619].
- [72] M. Rissee [Pierre Auger Collaboration], arXiv:astro-ph/0701065.
- [73] V. Berezinsky, M. Kachelriess and A. Vilenkin, Phys. Rev. Lett. **79**, 4302 (1997) [astro-ph/9708217].
- [74] V. A. Kuzmin and V. A. Rubakov, Phys. Atom. Nucl. **61**, 1028 (1998) [Yad. Fiz. **61**, 1122 (1998)] [astro-ph/9709187].
- [75] M. Birkel and S. Sarkar, Astropart. Phys. **9**, 297 (1998) [hep-ph/9804285].
- [76] P. Blasi, R. Dick and E. W. Kolb, Astropart. Phys. **18**, 57 (2002) [astro-ph/0105232].
- [77] S. L. Dubovsky and P. G. Tinyakov, JETP Lett. **68**, 107 (1998) [arXiv:hep-ph/9802382].
- [78] M. M. Winn, J. Ulrichs, L. S. Peak, C. B. Mccusker and L. Horton, J. Phys. G **12**, 653 (1986); see also the complete catalog of SUGAR data in “Catalog of highest energy cosmic rays No. 2”, ed. WDC-C2 for Cosmic Rays (1986).
- [79] M. Kachelriess and D. V. Semikoz, arXiv:astro-ph/0306282; H. B. Kim and P. Tinyakov, arXiv:astro-ph/0306413.
- [80] M. Teshima, private communication.
- [81] D. V. Semikoz and P. A. Collaboration, arXiv:0706.2960 [astro-ph].
- [82] R. Aloisio, V. Berezinsky and M. Kachelriess, Phys. Rev. D **74**, 023516 (2006) [arXiv:astro-ph/0604311].
- [83] J. R. Ellis, V. E. Mayes and D. V. Nanopoulos, Phys. Rev. D **74**, 115003 (2006) [arXiv:astro-ph/0512303].
- [84] Private communication with the authors of Ref. [83].
- [85] S. Sarkar, Acta Phys. Polon. B **35**, 351 (2004) [arXiv:hep-ph/0312223].